SUBSONIC WIND TUNNEL INVESTIGATION OF THE HIGH LIFT CAPABILITY OF A CIRCULATION CONTROL WING ON A 1/5-SCALE T-2C AIRCRAFT MODEL

Robert J. Englar

Naval Ship Research and Development Center
Bethesda, Maryland

May 1973

UNCLASSIFIED
Security Classification

AD- 781 856

DOCUMENT CONTROL DATA - R & D

Security classification of title, body of abstract and indexing annotation must be entered when the overall report is classified)

1 ORIGINATING ACTIVITY (*Corporate author*)
Aviation and Surface Effects Dept.
Naval Ship Research & Development Center
Bethesda, Maryland 20034

2a. REPORT SECURITY CLASSIFICATION
UNCLASSIFIED

2b GROUP

3 REPORT TITLE
SUBSONIC WIND TUNNEL INVESTIGATION OF THE HIGH LIFT CAPABILITY OF A CIRCULATION CONTROL WING ON A 1/5-SCALE T-2C AIRCRAFT MODEL

4 DESCRIPTIVE NOTES (*Type of report and inclusive dates*)
Technical Note

5 AUTHOR(S) (*First name, middle initial, last name*)
Robert J. Englar

6 REPORT DATE	7a. TOTAL NO OF PAGES	7b. NO OF REFS
May 1973	71	4

8a. CONTRACT OR GRANT NO	9a. ORIGINATOR'S REPORT NUMBER(S)
b. PROJECT NO	Technical Note AL-299
c. WF 421.212	9b. OTHER REPORT NO(S) (*Any other numbers that may be assigned this report*)
d. NSRDC 1690-120	

10 DISTRIBUTION STATEMENT
Approved for public release; distribution unlimited

11 SUPPLEMENTARY NOTES	12 SPONSORING MILITARY ACTIVITY
	Naval Material Command (03L4) Washington, D. C. 20361

13 ABSTRACT

A Circulation Control Wing, formed by the deflection of a 15-percent chord flap through 180 degrees to produce a circular cylinder trailing edge with tangential upper surface blowing, was applied to a 1/5-scale T-2C aircraft model. The flap span/wing span ratio was 0.495, consistent with the conventional aircraft. Subsonic investigations were conducted in the Naval Ship Research and Development Center (NSRDC) 8- by 10-foot North Wind Tunnel over a dynamic pressure range of 5 to 41 psf (Reynolds number based on mean aerodynamic chord of 0.60 to 1.68 million). Flap deflection was varied from 0 to 180 degrees, thus comparing the configurations of blown flap (moderate-to-high lift and lower drag for take-off) and the circular Coanda trailing edge (high lift and high drag for landing). At a Reynolds number of 1.43 million, a maximum lift coefficient of 3.33 was generated by the Circulation Control Wing at a momentum coefficient of 0.156, compared to $C_{L_{max}} = 1.70$ for the conventional aircraft with a 37-percent chord single slotted flap deflected 33 degrees. Performance was limited by part-span (as opposed to full-span) blowing and large vorticity generated at the blown - unblown junction of the wing.

DD FORM 1 NOV 65 1473 (PAGE 1)
S/N 0101-807-6801

UNCLASSIFIED
Security Classification

TABLE OF CONTENTS

LIST OF TABLES

LIST OF FIGURES

SYMBOLS

A_j	Jet slot area, ft^2
a_j	Velocity of sound in the jet, ft/sec
c	Undeflected airfoil chord, ft
c_1	Airfoil chord with flap deflected 180 degrees, ft
c_f	Flap chord, ft
C_D	Aircraft drag coefficient
$C_{D_{JT}}$	Drag coefficient due to horizontal component of jet thrust
C_L	Aircraft lift coefficient
$C_{L_{JT}}$	Lift coefficient due to vertical component of jet thrust
C_ℓ	Sectional lift coefficient
C_M	Aircraft pitching moment about the mean quarter-chord
C_R	Non-dimensional resultant of horizontal and vertical jet thrust components
C_μ	Jet momentum coefficient based on total undeflected wing area
h	Jet slot height, ft
$\dot{m}$	Jet mass efflux, slugs/sec
M_j	Jet Mach number
P_d	Wing duct (plenum) total pressure, psf
P_∞	Free stream static pressure, psf
q	Free stream dynamic pressure, psf
q_u	Uncorrected free stream dynamic pressure, psf
R	Universal gas constant, 1715 $ft^2/(sec^2\ °R)$
r	Trailing edge radius, ft
R_e	Reynolds number based on mean chord
S	Undeflected wing planform area, ft^2
T_d	Duct total temperature, °R
T_j	Static temperature in the jet, °R
V_j	Jet velocity, ft/sec

x	Distance from airfoil leading edge, ft
α	Incidence, degrees
α_w	Wing incidence, degrees
α_{FRL}	Effective incidence of the fuselage reference plane ($\alpha_w - 2°$), degrees
$\alpha_{FRL_{geo}}$	Geometric incidence of the fuselage reference plane, degrees
γ	Ratio of specific heats
δ_f	Flap deflection angle, degrees
δ_j	Jet deflection angle, degrees
δ_n	Leading edge deflection (nose droop), degrees
δ_{n_o}	Outboard leading edge deflection, degrees
ε	Solid blockage correction factor
ε_w	Average wing downwash angle at the tail, degrees

SUMMARY

A Circulation Control Wing, formed by the deflection of a 15-percent chord flap through 180 degrees to produce a circular cylinder trailing edge with tangential upper surface blowing, was applied to a 1/5-scale T-2C aircraft model. The flap-span/wing-span ratio was 0.495, consistent with the conventional aircraft. Subsonic investigations were conducted in the Naval Ship Research and Development Center (NSRDC) 8- by 10-foot North Wind Tunnel over a dynamic pressure range of 5 to 41 psf (Reynolds number based on mean aerodynamic chord of 0.60 to 1.68 million). Flap deflection was varied from 0 to 180 degrees, thus comparing the configurations of blown flap (moderate-to-high lift and low drag for take-off) and the circular Coanda trailing edge (high lift and high drag for landing). At a Reynolds number of 1.43 million, a maximum lift coefficient of 3.33 was generated by the Circulation Control Wing at a momentum coefficient of 0.156, representing a 96-percent improvement over the conventional aircraft with a 37-percent chord single slotted flap deflected 33 degrees. Performance was limited by part-span (as opposed to full-span) blowing and large vorticity generated at the blown-unblown junction of the wing.

INTRODUCTION

Considerable recent research into the application of tangential upper surface blowing to the bluff trailing edges of helicopter rotor blades (see Reference 1 for a partial bibliography) has led to the application of a similar scheme to fixed wing aircraft. Employing the well-known Coanda principle, the concept involves a jet of air remaining attached to a rounded trailing edge, initially acting as a boundary layer control, but primarily controlling the airfoil stagnation points and thus the circulation around it. The resulting very high circulation lift (very little of which is attributable directly to the jet thrust component) is attainable at momentum coefficients considerably less than those necessary for a jet flap or blown flap application. Use of the circulation control principle on carrier-based or STOL aircraft

is expected to yield considerable reduction in landing velocities, increased aircraft payload and wing loading (or reduced wing area), reduced landing and take-off distances, and high drag generation on approach. The generation of lift essentially independent of incidence implies increased visibility due to low approach angles of attack, and the availability of a blowing source provides an additional possibility for transonic maneuvering.

The Circulation Control Wing (CCW) modes of operation are shown in Figure 1, where a short chord (15-percent or less of the wing chord) flap is rotated through 180 degrees to form the cylindrical Coanda surface. In the intermediate mode, the wing becomes a blown flap where moderate-to-high lift is generated at relatively low drag (profile drag is frequently negative); this configuration is effective during take-off where high drag is undesirable. In the approach mode, the rounded trailing edge is formed, thus eliminating a sharp trailing edge and allowing increased circulation due to the forward movement of the previously limited aft stagnation point. The resulting high augmentation due to blowing is accompanied by high drag (an appreciable profile drag can be generated by large jet turning angles and mixing). The increased circulation produces a corresponding aft movement of the leading edge stagnation point. At these high lift conditions the sharp nose radii of modern high performance airfoils produce such high leading edge suction peaks that some type of leading edge device or blowing is mandatory to prevent laminar separation.

The primary objective of the present investigation was to determine the feasibility of the Circulation Control Wing concept as applied to a three-dimensional aircraft model. An initial verification of the concept had been provided by an in-house two-dimensional wind tunnel investigation of a NACA 66-210 airfoil modified so that it very closely resembled the lower configuration in Figure 1. Nose droop angles from 0 to 43.6 degrees were employed, but only the 180° Coanda flap position was available. Figures 2 and 3 present a brief summary of those results: Figure 2 indicates that a section lift coefficient of 5.4 was obtained at a blowing coefficient of 0.24 and 43.6° nose droop; this was slightly less than three times the lift of the conventional airfoil with a split

flap at 5 times the Reynolds number. Figure 3 maps the resulting maximum (at fixed C_μ) lift coefficients as functions of blowing coefficient, incidence and nose droop. These results were sufficient to encourage the application of a rotatable blown trailing edge flap to an existing aircraft model to investigate the three-dimensional performance of the Circulation Control Wing.

MODEL AND EXPERIMENTAL APPARATUS

A 1/5-scale model of the T-2C aircraft was available and appeared to be an excellent choice for the investigation. It had previously been modified to accommodate an air supply, and in addition, a full scale T-2C was available for possible modification and flight demonstration should the present results prove promising. A three-view of the T-2C is shown in Figure 4, while Table I gives pertinent geometric characteristics for the full scale aircraft (model values are 20 percent of the linear dimensions).

The T-2C model was modified so that the flapped area was as shown in Figure 5, and the model was installed in the NSRDC North Subsonic Tunnel as shown in Figure 6. Additional details relating to configuration design parameters; design rationale; model installation, test technique and apparatus; and data corrections and tares are presented in Appendix A. It should be mentioned that all coefficients in the data presented are referenced to the original undeflected model wing area of 10.2 square feet.

RESULTS AND DISCUSSION

In this initial investigation to determine the effects of a three dimensional flow field on the Circulation Control Wing concept, major emphasis was placed on the longitudinal characteristics of the model. Whereas side force, rolling moment, and yawing moment data were recorded at zero yaw angle, no deliberate investigation of lateral characteristics was undertaken. Furthermore, as strongly emphasized during original tests by North American Aviation on this particular T-2 wind tunnel model (Reference 2), there is a noticeable asymmetry in the wing which caused the right side to stall before the left.

Table 2 presents a detailed outline of the full test schedule. Early portions of the investigation were conducted to determine the more optimum of several leading edge configurations, and with this determined, the best configuration was tested to determine the effects of blowing on lift augmentation, flap rotation from 0 to 180 degrees, and Reynolds number. This data was all run with horizontal tail off but with the vertical tail installed. Additional runs were made with the horizontal tail installed to determine control effectiveness in pitch. Finally, static tests (no dynamic pressure) were run at the five flap angles to determine the horizontal and vertical force components of the jet thrust.

LIFT AUGMENTATION AND CONFIGURATION IMPROVEMENT

The standard T-2C aircraft in the cruise mode (but without horizontal tail and without blowing) was run as a baseline configuration and data checkout case. Comparison to data from Reference 2 was quite good. This unblown data, as well as that for several additional unblown configurations including the conventional landing mode, is shown in Figure 7. The trailing edge was then converted to the 180° Coanda configuration, and excellent Coanda turning was exhibited statically as shown by the tuft in Figure 8. (At this point in the investigation, the flow fence and leading edge droop shown in this figure were not installed.)

A series of runs was conducted for several selected incidences at a dynamic pressure of 30 psf (Reynolds number of 1.43×10^6 based on a mean undeflected chord of 1.48 feet). Figure 9 shows the variation in lift with blowing at constant geometric fuselage incidence. (Actual incidence is higher due to the correction for tunnel boundary restriction. Wing geometric root incidence is +2 degrees relative to the fuselage reference line, and a twist of -3° about the quarter chord is present.) The typical behavior of lift with blowing was seen for geometric incidence of 4 degrees or less, i.e., rapid initial lift rise due to boundary layer control followed by less rapid but continuous increase due to supercirculation. However, at the higher angles of attack, some lift decrease with C_μ was observed. This was

thought to be due to leading edge laminar separation, which had been shown by surface static pressure distributions to occur in the two-dimensional tests. Thus, the leading edge corresponding to the flapped wing area was drooped 30 degrees, and Figure 10 resulted. The low incidence curves practically repeat Figure 9, but 8° and 12° data show definite improvement. This configuration was also run over an angle of attack range at constant C_μ. The resulting lift, drag, and moment data are shown in Figure 11, as are several cross-plotted points from Figure 9 for the undrooped leading edge. The stall angle with blowing always fell between 10 and 11 degrees. Reference 2 showed the stall of the conventional aircraft with flaps deployed to be between 13 and 14 degrees, and even the unflapped wing stalled at 14 degrees. Furthermore, the unblown data of Figure 7 shows that the 30° nose droop can extend the stall to roughly 17 degrees. It was clear that stall with blowing was occurring prematurely, but the reason was uncertain.

Small cotton tufts were attached to the wing upper surfaces in an attempt to visualize the existing flow field. Figure 12 depicts the results with and without blowing. At 0 and 8 degrees incidence, blowing has the effect of entraining flow in a spanwise direction from the unblown outboard section; the tufts on the ailerons turn drastically inboard. No upper surface separation exists. At 12 degrees, no separation exists for the unblown case (Figure 11 shows this to still be below stall), but the blown case shows the entire outboard section completely separated, with a strong influence being felt near midchord of the blown section (Figure 11 shows this data to be well beyond stall). The last two pictures of Figure 12 show strong separation for both cases, although lift drop-off does not occur for the unblown case. Premature stall was thus strongly confirmed for the blown case.

It was hypothesized that this phenomenon was being caused by a very strong vortex formed by the large spanwise discontinuity in lift between the blown and unblown sections, and thus a low aspect ratio, high lift wing was being produced inboard of this junction. Furthermore, this effective tip vortex should roll up in the conventional sense, inducing severe upwash angles on the outboard section. This

section would then stall below its normal geometric stall angle, and the stall would propagate inboard. The tuft pictures seemed to verify this, but it was desired to confirm it. A neutrally bouyant helium bubble generator was installed in the tunnel upstream of the junction, and many pictures similar to Figure 13 were taken. The strong vorticity is evident. Other pictures from the side showed downwash angles at the trailing edge which approached 30 degrees or more, and top views showed vortex inwash angles (towards the fuselage) of perhaps 15 to 20 degrees. An obvious remedy would be extension of the blown trailing edge out to the wing tip, thus eliminating outboard stall due to vortex upwash and removing the vortex influence from the inboard section (where it was reducing the incidence). However, for this initial investigation it was desired to maintain the same flapped area as the original aircraft.

As an alternative, the flow fences seen in Figures 6 and 8 were applied to separate the blown and unblown sections, and an outboard leading edge droop of 10 degrees was added to delay the stall. (The abruptness of the stall in Figure 11 indicated that it was of the leading-edge type). Figure 14 shows the resulting improvement: an increase of 7 to 8 degrees in stall incidence and 0.65 in $C_{I_{max}}$ at $C_\mu = 0.156$. That the vortex is still present and strong is shown by Figure 13, which was taken of this configuration. The absence of a noticeable change in blown lift curve slope between Figures 11 and 14 indicates little change in effective aspect ratio. However, the tuft pictures of Figure 15 show much less inwash towards the blown section, and no influence inboard when the outboard panel stalls at 17.5°. Figure 16 shows the lift, drag, and moment variation with C_μ at constant incidence (both geometric and actual), where no lift drop off is seen at any angle. It was thus decided to use Configuration 4 ($\delta_f = 180°$, $\delta_n = 30°$, $\delta_{n_o} = 10°$, fences) as the baseline for the remainder of the test.

Mention should be made concerning the experimental relationship of C_μ to plenum pressure. Figure 17 depicts both calculated and

measured mass flux ($\dot{m}$) and C_μ as functions of wing plenum pressure. The dashed curves were calculated using the isentropic equations (see Appendix A) and a slot area per plenum of 0.424 in.^{2} (based on a measured mean slot height of 0.0212 inch and length of 20.0 inches). It was noted that the slot height expanded under pressure due to the thin knife edge which formed the slot upper surface. Measurement of this expansion at P_d = 40 in Hg. showed an increase of 45 percent in slot area; the measured mass flow at the same pressure in Figure 17 is nearly the same percentage greater than the calculated value. Using the increased area in the isentropic calculation would cause the curves almost to coincide; the difference would be due to non-isentropic losses in the nozzle.

BLOWN FLAP ROTATION

To convert from the cruise to the landing configuration of Figure 1, the trailing edge flap would be required to deflect through 180 degrees. It was thus necessary to investigate intermediate flap angles both with and without blowing. Figures 18 through 21 present lift, drag, and moment data at constant flap angle, and together with Figure 14 give the characteristics of the system in operation between 0 and 180° at 45 degree increments. For flap deflection of 90° and greater a lift coefficient of 3.0 or greater is generated for C_μ between 0.154 and 0.162. Drag produced in all three cases is high, ranging from C_d = 1.08 to 1.12 at maximum C_L. These data show excellent promise in landing operation, compared to the standard T-2C with C_d = 0.32 at $C_{L_{max}}$ = 1.7 (Figure 7). It is interesting to note from the drag polars that for the higher blowing cases for $\delta_f \geq 90°$, stall is accompanied by a reduction in drag instead of the usual increase. The tail-off pitching moments are negative and relatively large with blowing due to the high trailing edge suction peaks produced by the jet.

For the take-off mode, Figure 20 shows the 45-degree blown flap to be promising, with somewhat lower C_L than above, but at much

reduced drag coefficients. The strong thrust contribution of the jet is partially responsible, as is reduced trailing edge suction and decreased induced drag. Negative pitching moment is also reduced due to reduced suction peak and re-direction of the thrust vector. The cruise mode ($\delta_f = 0°$) data in Figure 21 shows relatively small lift augmentation, but drag reduction which could prove useful in cruise. Note that in certain cases drag reduction is nearing 90% of the momentum flux, indicating good thrust recovery. An additional benefit of this configuration could be in transonic maneuverability.

A summary comparison of the above data for different flap angles at $C_\mu \simeq .156$ is shown in Figures 22 and 23, where the standard T-2C flapped configuration from Figure 7 is included for reference. The relatively high L/D of the 45° flap case shows its take-off potential while the low L/D at high C_L for flap angles of 90° to 180° displays the landing potential.

In the preceding data, relatively little difference was seen between the 90° and 180° flap configuration at the higher blowing rates. This was unexpected, based on existing two-dimensional data comparing blown flap and Circulation Control airfoils. Figure 24 depicts a large compilation of two-dimensional blown flap data from Reference 3, as well as some data for the elliptic Circulation Control rotor airfoil of Reference 4 and the previously mentioned CCW configuration of the NACA 66-210 airfoil. For both bluff trailing edge airfoils, incremental C_L values of 2 or more were achieved with considerably less blowing than for the same lift from a 15-percent chord blown flap. With respect to net lift due to blowing, a comparison of Figures 14 and 19 can be misleading, since the unblown lift values of the 90° flap case are considerably larger due to the high camber. Incremental $C_{L_{max}}$ as a function of blowing for the five flap angles is shown in Figure 25, where for $C_\mu \simeq 0.156$, the Coanda trailing edge produces an additional 0.36 in $\Delta C_{L_{max}}$, roughly a 22-percent increase. A similar trend in lift augmentation is seen in Figure 26. Note that while

lift increases with C_μ, the augmentation (incremental lift divided by momentum flux) decreases; maximum blowing effectiveness occurs at the low C_μ values, which are primarily in the boundary layer control regime.*

It is felt, based on two-dimensional results, that the lift augmentation of the 180° flap configuration should be significantly higher than it is in proportion to the 90° flap, and that a significant influence upon it is being caused by the midspan vortex. No flow fences had been installed other than those shown in Figure 6 or 8; i.e. the Coanda surface and fully deflected flap were not shielded from the vortex rollup. For the 90° flap, the jet kinetic energy is still relatively high when it reaches the flat upper surface of the flap, and is shielded from the oncoming vortex by the flap itself. It is surmised that detrimental effects of the vortex would thus be considerably less than for the 180° case. For the 180° configuration, the jet possesses much less energy when it turns into the oncoming vorticity; the balance of centrifugal force and surface suction which maintains jet attachment is thus considerably more delicate at this point. In addition, no shielding flap is present, and it is thus felt that the three-dimensional effects of the vortex are much more severe. This is somewhat verified by a slight reduction (.016/degree) in lift curve slope (lower effective aspect ratio) for the fully deflected flap. Full span blowing should considerably alter this condition, but in the present case of part span blowing, it is proposed that a large fence be added to the blown trailing edge and to the wing undersurface for all configurations.

---

*It is in this regime of maximum augmentation that the CCWing would be operating if applied to a standard T-2C with existing engines. The twin J-85 engines are capable of a maximum of 6 percent bleed (5.28 lbs/sec, total), which at a pressure ratio $P_d/P_\infty = 3.0$, yields a momentum coefficient $C_\mu = 0.843/q$. For approach dynamic pressures of 20 to 30 psf (77 to 94 knots), this produces C_μ values of 0.042 to 0.028 respectively.

STATIC JET THRUST COMPONENTS

A brief mention of the contribution of the jet thrust component to lift and drag is in order. Jet flap data is frequently broken down into a circulation lift component and a jet reaction component ($C_\mu \sin \delta_j$), where the latter term is a very significant one at high blowing rates. Horizontal and vertical force components acting on the model were measured with no freestream dynamic pressure and the model at -2° (zero wing incidence). These components were then nondimensionalized by the q S (30 x 10.2) at which the entire investigation (except Reynolds number cases) was run to yield an effective lift and drag coefficient due to jet thrust. These are plotted as a function of the corresponding C_μ in Figures 27 and 28. Note that even for the 90° flap the lift component is quite small relative to the total C_L of Figures 14, and 18 through 21. This indicates a basic and significant difference between Circulation Control and jet flaps: the latter achieves a large portion of its net left from the vertical component of jet thrust, whereas the CC Wing is primarily a circulation augmenter. The following table demonstrates the degree of jet turning over the Coanda surface for a sample $C_\mu = 0.10$; C_R is the nondimensional resultant force coefficient acting 180° from the angle δ_j:

δ_f	$\delta_{f_{\text{upper surface}}}$	δ_j calculated	C_R
0°	8.25°	5.23°	.0989
45	53.25	53.62	.1025
90	98.25	97.33	.0713
135	143.25	153.97	.0479
180	188.25	177.50	.0530

The jet turning angles are close to the actual upper surface deflections, indicating good Coanda effect; C_R is close to C_μ for 0 and 45° (indicating almost full thrust recovery) but begins to decrease with additional turning. (There appears to be some discrepancy in the 135° data, possibly due to inaccuracy in recording the very small forces involved.)

REYNOLDS NUMBER VARIATION

A range of dynamic pressures was run for two configurations, each at a constant geometric incidence. Figure 29 depicts the lift variation for Configuration 3 of Figure 11 at $\alpha_{FRL_{geo}} = +8°$ and Reynolds number from 0.60 to 1.68 million. For $C_\mu \leq 0.09$, increase in Reynolds number produces an increase in lift for constant blowing. Above $C_\mu = 0.09$, comparison of the curves is less meaningful. This is because the actual incidence does not remain constant due to tunnel boundary effects ($\alpha_{FRL} = \alpha_{FRL_{geo}} + 0.965\ C_L$), and thus the true angle eventually exceeds the stall incidence. A similar trend was displayed for Configuration 4 (from Figure 14), where Reynolds number increase again yielded increased lift coefficient, indicating possible additional lift payoff for a full scale vehicle. However, the percentage gain appeared less at higher Reynolds number.

TAIL-ON LONGITUDINAL CHARACTERISTICS

A series of horizontal tail-on data was run for flap deflections of 90° and 180°, with zero tail incidence and dynamic pressure of 30 psf. The results are shown in Figures 30 and 31 for three values of C_μ. Trim is achieved at all blowing rates for $\delta_f = 180°$ with elevator deflection between -11 and +2 degrees; trim $C_{L_{max}}$ for the highest blowing rate is 6 percent less than the tail-off maximum. An insufficient number of elevator deflection angles to determine the trim range were run for the $\delta_f = 90°$ case, but by extrapolation from Figure 31, the values appear close to that for the 180° case.

It is interesting to note for both flap deflections at higher blowing the effect of the high downwash angles on the tail with negative elevator deflection. The inverted cambered section is then operating at a high incidence, and the nose-up moment produced by the tail down load dominates the nose-down moment from the wing trailing edge suction peak. The result for $\delta_f = 180°$, $\delta_e = -10°$, and $C_\mu = 0.156$

is almost neutral stability (Figure 30.) At this blowing rate, the horizontal tail surfaces stall negatively at low fuselage incidence ($\alpha_{FRL} \leq 4°$) due to the large downwash angles.

As only one value of tail incidence ($i_t = 0°$) was run, an insufficient amount of data was generated to evaluate the average downwash angle at the tail from the intersections of the tail-on and tail-off C_M versus C_L curves except at one point for each flap angle. Both points were for $C_\mu = 0$. They are obviously not upper limits, and from the helium bubble pictures taken, values of 30° or more are expected. Additional values of tail incidence will have to be set during future testing to determine the actual limiting values.

Figure 32 indicates the effect of blowing on stability for tail on and off at two flap angles. These values are the slope of the lift-moment curves at $C_L = 0.75\ C_{L_{max}}$, at which point the curves were essentially linear. It is seen that increased blowing tends to be stabilizing for the tail-off curves. Tail-on data shows stability for all C_μ values tested, although decreasing with higher blowing.

• CONCLUSIONS AND RECOMMENDATIONS

Subsonic wind tunnel investigations conducted on a 1/5-scale T-2C model with a Circulation Control Wing have shown the feasibility of the concept in generating high lift and drag on approach, and somewhat lower lift at significantly reduced drag on take-off. Experimental data obtained for the model over a range of incidence, momentum coefficient, flap deflection angle, and Reynolds number yielded the following conclusions:

- Lift coefficients of 3.33 at $C_D = 1.08$ were generated for $C_\mu = 0.156$ at $\delta_f = 180°$, representing a 96% increase in lift and 240% increase in drag over the conventional ($\delta_f = 33°$) T-2C unblown values. For take-off, $C_L = 2.90$ and $C_D = 0.56$ were generated at the same blowing and 45 degrees flap deflection.

- Due to the strong spanwise discontinuity in lift between the blown and unblown wing sections, severe vorticity formed at this junction and caused a greatly reduced effective aspect ratio. The resulting upwash caused premature separation outboard and influenced the inboard characteristics in spite of partial fences installed between the sections.

- The effectiveness of the 180° and 135° flap deflections compared to the 90° case was not as great as predicted from previous 2-D results. It is felt that the first two cases were more strongly affected by the above mentioned vorticity and were not operating at maximum effectiveness. Nevertheless, even though maximum lift coefficient attainable was similar for 90 and 180° flap deflection, lift augmentation due to blowing was noticeably better for the full Coanda trailing edge.

- Increased Reynolds number was seen to increase lift at constant C_μ, thus indicating additional increased performance for a full scale flight demonstrator.

- At the highest lift experienced, the present model could still be trimmed with existing elevator deflections, and only 6-percent or less of $C_{L_{max}}$ was lost due to download on the tail. Downwash angles at the tail appear to be large.

The following recommendations are suggested by the present investigation:

- Installation of lower surface and trailing edge fences is necessary to separate the blown section from the adverse effects of the induced vorticity. Even more desirable would be conversion to full span blowing.

- Future investigations need be conducted in a larger facility to eliminate wall boundary effects.

- Additional investigations should be run over a larger range of elevator deflections and additional tail incidences.

- Lateral characteristics with blowing should be investigated, including roll generated by differential blowing.

ACKNOWLEDGMENT

The author wishes to express his appreciation to the Subsonic Wind Tunnel crew of the NSRDC Aviation and Surface Effects Department for their valuable assistance during the present investigation, which was run in March-May 1973. Appreciation is also due to Mr. J. Ottensoser for the effort involved in converting the original T-2J model into the present T-2C configuration.

REFERENCES

1. Stone, Michael B. and Robert J. Englar, "Circulation Control - A Bibliography with Selected References," Naval Ship Research and Development Center Report 4108, (Jul 1973).

2. Cohen, M. H. and J. K. Kagawa, "Low Speed Wind Tunnel Tests of a 0.20-Scale Model of the T2J-1 Airplane to Determine General Aerodynamic Characteristics and Duct Pressure Recovery Data," Los Angeles, Calif., North American Aviation Inc. Rpt NA-56-1296 NAA-358, Vol. 2 (Sep 1957).

3. Riebe, John M., "A Correlation of Two-Dimensional Data on Lift Coefficient Available with Blowing-, Suction-, Slotted-, and Plain-Flap High Lift Devices," NACA RM L55D 29 a (Oct 1955).

4. Williams, Robert M. and Harvey J. Howe, "Two-Dimensional Subsonic Wind Tunnel Tests on a 20 Percent Thick, 5-Percent Cambered Circulation Control Airfoil", Naval Ship Research and Development Center Tech Note AL-176 (AD 877-764) (Aug 1970).

APPENDIX A

MODEL, EXPERIMENTAL APPARATUS, AND TECHNIQUE

MODEL

The present 1/5-scale model T-2C had been modified for an air supply during previous studies but remained essentially the same as the standard aircraft with the exception of the flap area. For this investigation, the standard 37-percent chord slotted flaps were removed, as was the area immediately forward of them bounded by the wing main spar. In place of this were installed the wing plenum chambers and the 15-percent chord flap, which could be deflected from 0 to 180° in 45 degree increments by installation of wedge-shaped spacers. Details of the plenum and flap arrangement are shown in Figure 5, where the very important trailing edge parameters (r/c, h/r, x/c_{slot} and tangency at the slot exit) were chosen based on the previous two-dimensional tests. These variables were in turn based on a limiting range of values which were known empirically to produce effective Coanda performance. The flap chord length of 15-percent was chosen as that needed to produce the geometric parameters of Figure 5. (Aft slot location is desirable for good performance at low incidence, but a slot too far aft results in poor BLC and thus upper surface separation). When fully rotated the flap only reduced the chord by 11.4 percent, and the total wing area was only reduced by 6.0 percent. The flap span/wing semi-span ratio remained at 0.495, consistent with the original slotted flap configuration. All coefficients in the presented data are referenced to the original undeflected model wing area of 10.2 square feet.

The model wing plenums were instrumented with a total pressure pickup in each, a thermocouple in the right chamber. Each plenum was 7/8" O.D. copper tubing and high pressure temflex tubing to a steel supply cylinder located within the model lower fuselage assembly. Internal dimensions of the cylinder were 7.80 inches in length and 2.75 inches in diameter, and total pressure and temperature pickups were installed in the aft end. As there was no provision made for individual pressure adjustment between left and

right wing plenums, care was exercised in setting the plenum slot heights using the adjustment screws shown in Figure 5. Any differences could be monitored by the separate pressure pickups. As the supply cylinder occupied the internal fuselage, no flow-through ducting simulation was possible; the engine inlets were thus faired smoothly into the body (see Figure 6).

TEST APPARATUS AND TECHNIQUE

The three-dimensional investigation was conducted in the Naval Ship Research and Development Center's 8- x 10-foot North Subsonic Tunnel. The model was mounted on a main strut and a pitch strut as shown in Figure 6 with the 7.55 foot wing span located horizontally in the 10 foot width of the tunnel. Air was supplied to the model through 1.5-inch I.D. flexible tubing which ran up through the tunnel balance frame and connected to the steel supply cylinder in the model. Mass flow into the model was measured by a venturimeter located in a supply line; the system was capable of a maximum of 2 lbs/sec flow.

Six-component data from the balance frame were recorded by strain gage flexures located on Toledo mechanical balances attached to the frame. The strain gage signals were fed into and processed by a Beckman 210 High-Speed Data System, which digitized and recorded them on magnetic tape for later reduction on an XDS-930 digital computer. For each data point, the Beckman system recorded all data 10 times over a 10 second interval (to denote any unsteadiness), and then took the average of those. Data from the Toledo scales were automatically recorded for each data point, and were punched on paper tape as a check on the electrical data system.

The jet momentum (blowing) coefficient was calculated as:

$$C_\mu = \frac{\dot{m} V_j}{q S}$$

where the mass flux ($\dot{m}$) was recorded by the venturimeter and the jet velocity was calculated assuming an isentropic expansion from wing plenum total conditions to freestream static conditions:

$$V_j = a_j M_j = \sqrt{\gamma RT_j}\, M_j = \left\{ 2\, RT_d \left(\frac{\gamma}{\gamma - 1} \right) \left[1 - \left(\frac{P_\infty}{P_d} \right)^{\frac{\gamma - 1}{\gamma}} \right] \right\}^{1/2}$$

It is realized that expansion to local static conditions at the jet exit gives a far more realistic value of V_j, and that expansion to free-stream static pressure underestimates V_j and M_j. However, local exit conditions are functions of local geometry, and thus a comparison of two blown airfoils of unlike trailing edge geometry but identical mass flows and plenum pressures would yield unlike values of C_μ. The momentum coefficient based on expansion to freestream conditions is thus accepted as a more "universal" parameter for comparison of blown systems. Similarly, isentropic mass flow was calculated as a check on the venturimeter as follows:

Choked flow: $$\dot{m} = A_j P_d \sqrt{\frac{\gamma}{RT_d}} \left(\frac{2}{\gamma + 1} \right)^{\frac{\gamma + 1}{2(\gamma - 1)}}$$

Unchoked flow: $$\dot{m} = A_j P_d \left\{ \frac{2\gamma}{(\gamma - 1)RT_d} \left[\left(\frac{P_\infty}{P_d} \right)^{2/\gamma} - \left(\frac{P_\infty}{P_d} \right)^{\frac{\gamma + 1}{\gamma}} \right] \right\}^{1/2}$$

TARES AND DATA CORRECTIONS

Wind-off weight tares were recorded for each configuration over the expected angle of attack range, and these values were subtracted from the wind-on data. To account for any additional effect on the balance due to pressure in the air supply line, a series of pressure tares was also run. The temflex supply hoses were disconnected at the wing plenums and plugged. A range of pressures covering the desired C_μ range was then run and the results on the balance recorded and correlated with static pressure measured in the main supply line just below the balance frame. These data were subtracted from the wind-on

data based on the supply line static pressure recorded with the wing plenums reconnected.

Solid blockage corrections to dynamic pressure were calculated as

$$q = q_u (1 + 2\varepsilon)$$

where $\varepsilon = 0.00561$ was based on blocked area due to fuselage, wings, mounting strut, and tip tanks. Uncorrected dynamic pressure was measured by calibrated piezometer ring differential read on a $\pm$ 1.0 psid transducer. The following tunnel boundary corrections were applied:

$$\Delta\alpha = 0.965\ C_L, \text{ degrees}$$

$$\Delta C_D = 0.0167\ C_L^2$$

$$\Delta C_M = 0.0182\ C_L$$

where the moment correction was applied only with the horizontal tail installed. To insure that tunnel flow breakdown did not occur from impingement of the jet sheet on the floor, rows of cotton tufts were taped to the floor in the vicinity of the model trailing edge - these were never seen to be affected by the jet flow field.

TABLE 1 - GEOMETRIC CHARACTERISTICS OF THE T-2C AIRCRAFT

Full Scale Dimensions (Model Factor = 0.20)

Wing	
Area, ft^2	255.0
Span, ft. (including tip tanks)	37.77
Aspect ratio	5.0
Taper ratio	0.50
Chords: root (Wing Sta. 0.00), in.	114.20
tip, in.	57.09
M.A.C. (Wing Sta. 95.255), in.	88.86
Fus. Sta. of .25$\bar{c}$, in.	216.7
M.A.C. height above Fus. Ref. Plane, in.	6.12
Airfoil section: root and tip	NACA 64A212 modified
Dihedral, deg.	+3.00
Incidence of root chord, deg. from Fus. Ref. Plane	+2.00
Aerodynamic twist, deg.	-3.00
Element about which wing is twisted, % c	25
Sweepback angle of 25% elem., deg.	2.28
Flap (Conventional T-2C)	
Type	Single Slotted
Area (total), ft^2	50.0
Span (one side), in.	102.5
Root chord, in.	39.5
Tip chord, in.	29.5
Flap (Circulation Control Wing)	
Area (total), ft^2	20.1
Span (one side), in.	102.5
Root chord, in.	16.2
Tip chord, in.	12.1

TABLE 1 - Continued

Horizontal Tail		
Area, ft^2		58.0
Span, ft.		16.43
Aspect ratio		4.5
Taper ratio		0.5
Chords:	root (H.T.Sta. 0.00), in.	58.4
	tip	29.52
	M.A.C. (H.T. Sta. 43.80), in.	45.40
	Fus. Sta. of $.25\bar{c}_h$, in.	422.35
	M.A.C. height above Fus. Ref. Plane, in.	57.20
Airfoil Section root and tip		NACA 65A012
Fuselage		
Overall length, ft.		38.7
Overall length excluding tail, ft.		34.2
Maximum diameter, ft.		4.45
Fineness ratio		8.05

TABLE 2 - T-2C CIRCULATION CONTROL WING TEST PROGRAM

NSRDC 8 X 10-FOOT SUBSONIC NORTH TUNNEL

Run No.	Con-fig.	δ_{flap}	$\delta_{n_{inb'd}}$	$\delta_{n_{outb'd}}$	$\delta_{elevator}$	Flow Fences	α_{FRL}	P_{duct} in. Hg.	q_{psf}	Purpose
2	1	0	0	0	Off	Off	-4 → 17	0	30	Standard Aircraft
34-48	2	180	0	0	Off	Off	-4,0,4,8,12	0 → 52	30	High Lift Capability
18-33	3	↓	30	↓	↓	↓	↓	↓	↓	(C_L - C_μ Ranges)
62-67	4	↓	↓	-10	↓	On	-4,0,8,12,15	↓	↓	↓
49-52	3	180	30	0	Off	Off	-4 → 20	0,15,30,52	30	Blown Flap Rotation
58-61	4	↓	↓	-10	↓	On	↓	↓	↓	↓
91-92	7	90	↓	↓	↓	↓	-4 → 17	↓	↓	↓
93-94	8	135	↓	↓	↓	↓	-4 → 18	↓	↓	↓
95-96	9	45	↓	↓	↓	↓	-4 → 17	↓	↓	↓
97	10	0	↓	↓	↓	↓	-4 → 18	↓	↓	↓
53	3	180	30	0	Off	Off	8	0 → 52	40	Reynolds No.
54	↓	↓	↓	↓	↓	↓	↓	↓	30	Variation
55	↓	↓	↓	↓	↓	↓	↓	↓	20	↓
56	↓	↓	↓	↓	↓	↓	8,4	↓	10	↓
57	↓	↓	↓	↓	↓	↓	↓	↓	5	↓
68	4	180	30	-10	Off	On	14	0 → 52	40	↓
69	↓	↓	↓	↓	↓	↓	↓	↓	30	↓
71,73	↓	↓	↓	↓	↓	↓	14,12	↓	20	↓

TABLE 2 - T-2C CIRCULATION CONTROL WING TEST PROGRAM (continued)

NSPDC 8 X 10-FOOT SUBSONIC NORTH TUNNEL

Run No.	Con-fig.	δ_{flap}	$\delta_{n_{inb'd}}$	$\delta_{n_{outb'd}}$	$\delta_{ele-vator}$	Flow Fences	α_{FRL}	P_{duct} in. Hg.	q_{psf}	Purpose
70,72	4	180	30	-10	Off	On	14,12	0 → 52	10	R_e Variation
80-82	5	180	30	-10	-10	On	-4 → 18	0,15,52	30	Elevator Effectiveness
75-77					0					
78-79					+5					
85-86					+15					
83					+20			52		
87,88	6	90			0		-4 → 17	0,15,52		
89					+20					
48S	2	180	0	0	Off	Off	-2	0→52	0	Static Thrust
92S	7	90	30	-10		On				
94S	8	135								
96S	9	45								
97S	10	0								
1	1	0	0	0	Off	Off	-4,8,20	0	0	Weight Tares
3-10	2	180	0	0	Off	Off		0→50		
11-17	3,4		30	0,-10	Off	Off, On	-4,6,16			
74+,84+	5	180	30	-10	On	On				
84+	6	90								

TABLE 2 - T-2C CIRCULATION CONTROL WING TEST PROGRAM (concluded)

NSRDC 8 X 10-FOOT SUBSONIC NORTH TUNNEL

Run No.	Con-fig.	δ_{flap}	$\delta_{n_{inb'd}}$	$\delta_{n_{outb'd}}$	$\delta_{ele-vator}$	Flow Fences	α_{FRL}	P_{duct} in. Hg.	q_{psf}	Purpose
90+	7,8,9,10	90,135,45,0	30	-10	Off	On	-4,6,16	0→50	0	Weight Tares
	3	180	30	0	Off	Off	)→13	0→30	30	Tuft Studies
	4	180	30	-10	Off	On	0→19	0,25	20	↓
	4	180	30	-10	Off	On	0°	15	5,20	Flow Visualization Bubble Generator

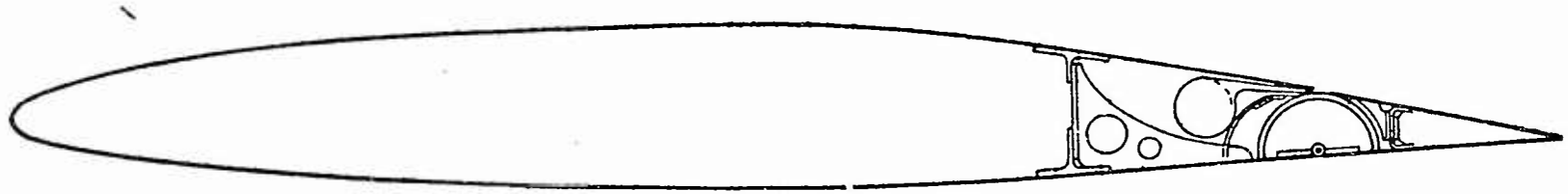

CONVENTIONAL (LOW LIFT AND DRAG COEFFICIENTS) IN CRUISE

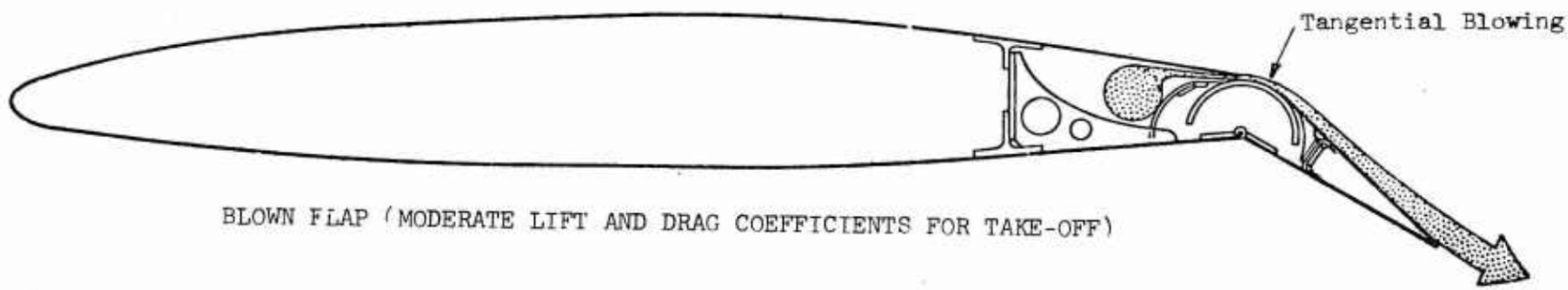

BLOWN FLAP (MODERATE LIFT AND DRAG COEFFICIENTS FOR TAKE-OFF)

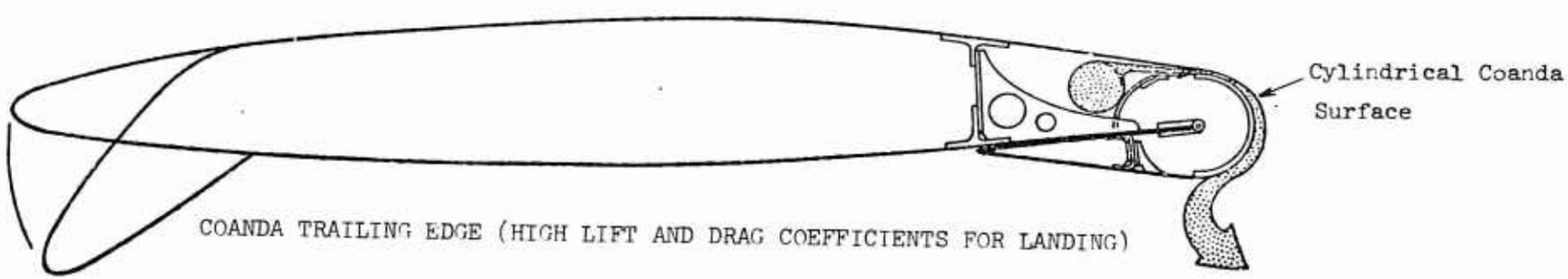

COANDA TRAILING EDGE (HIGH LIFT AND DRAG COEFFICIENTS FOR LANDING)

Figure 1 · Circulation Control Wing Modes of Operation

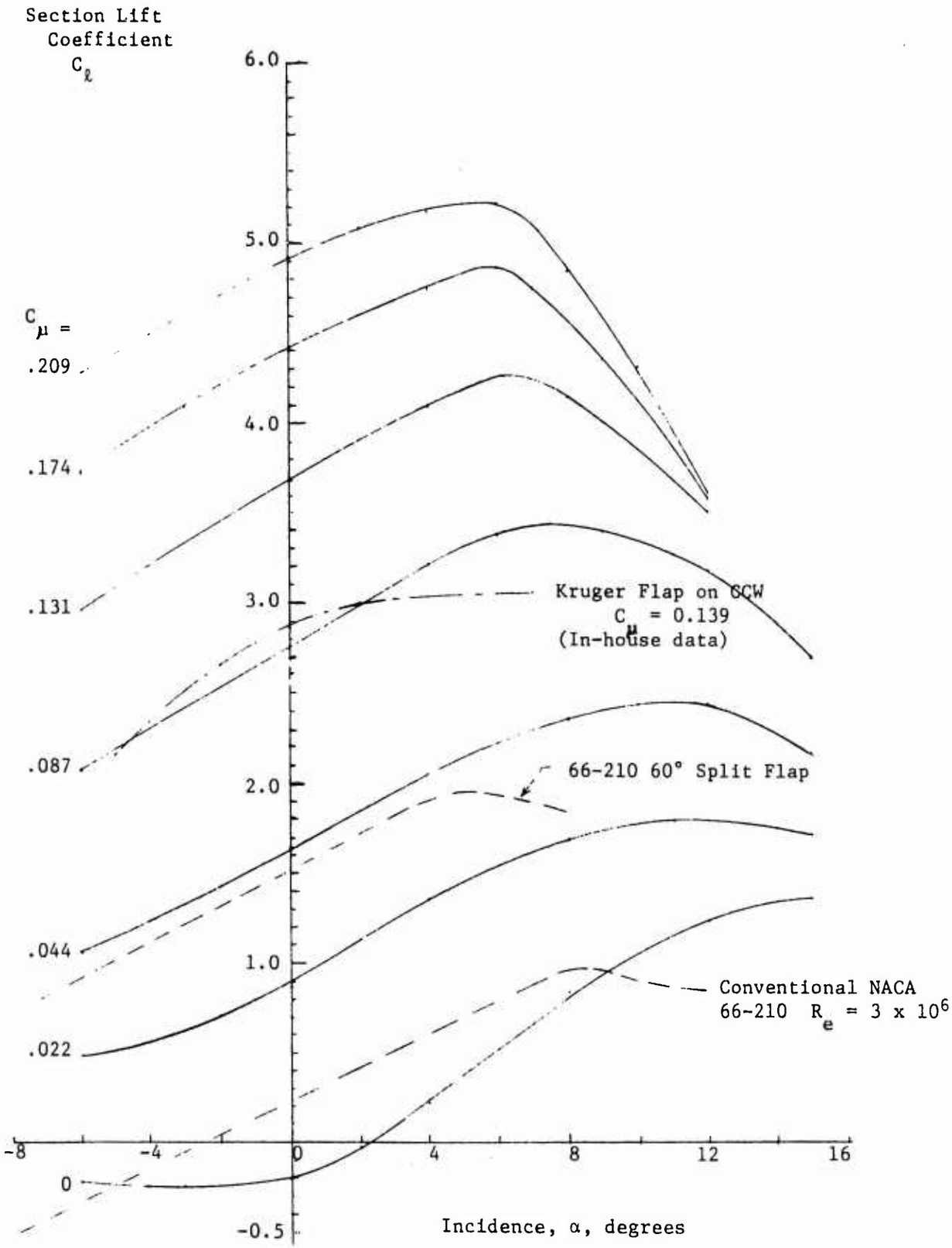

Figure 2 - Lift Characteristics of a Two-Dimensional Circulation Control Trailing Edge Applied to a NACA 66-210 Airfoil with 43.6° Nose Droop

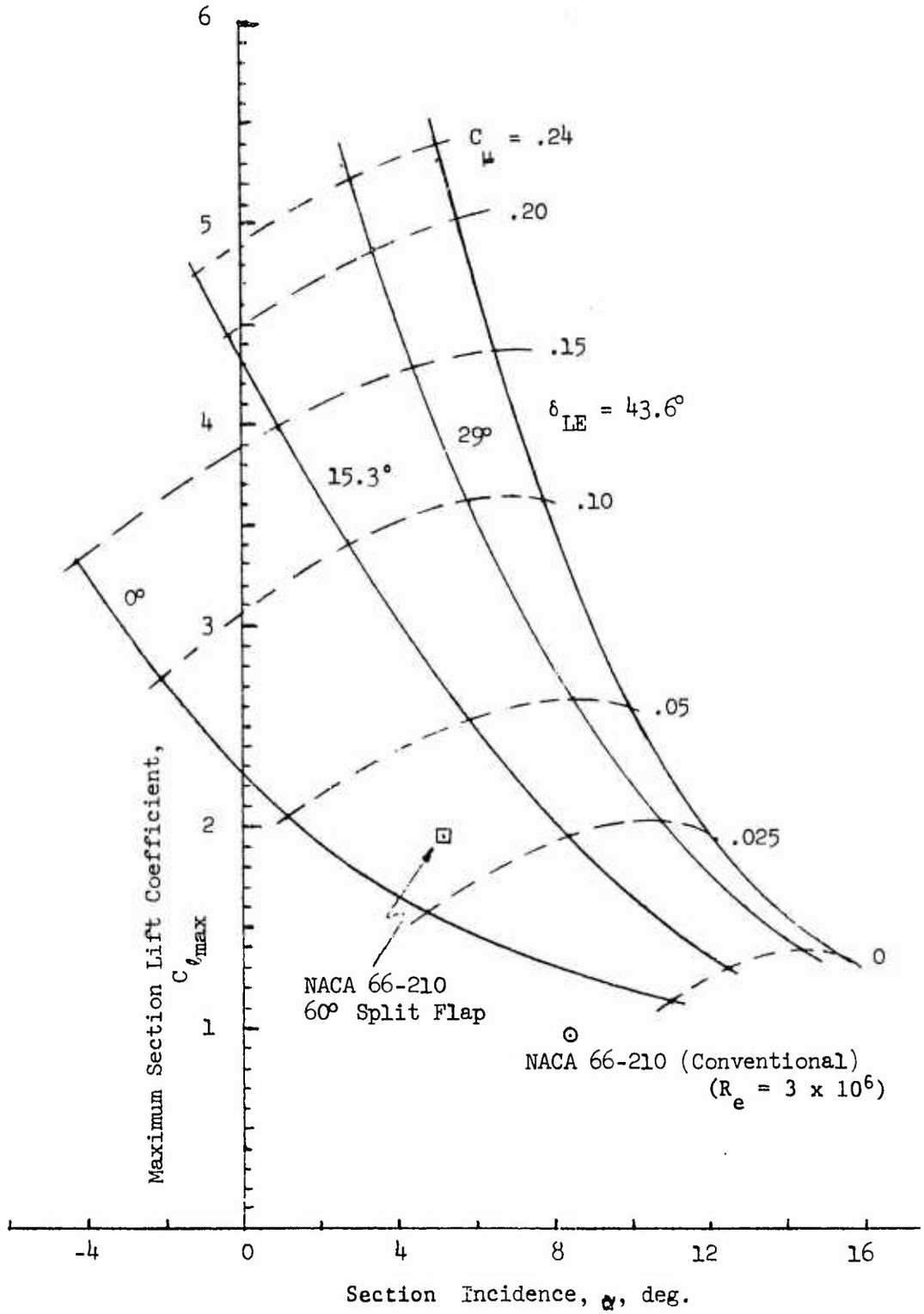

Figure 3 - Maximum Lift Attainable at Constant Blowing on a Two-Dimensional Circulation Control Trailing Edge Applied to a NACA 66-210 Section (R_e = 0.5 x 10^6)

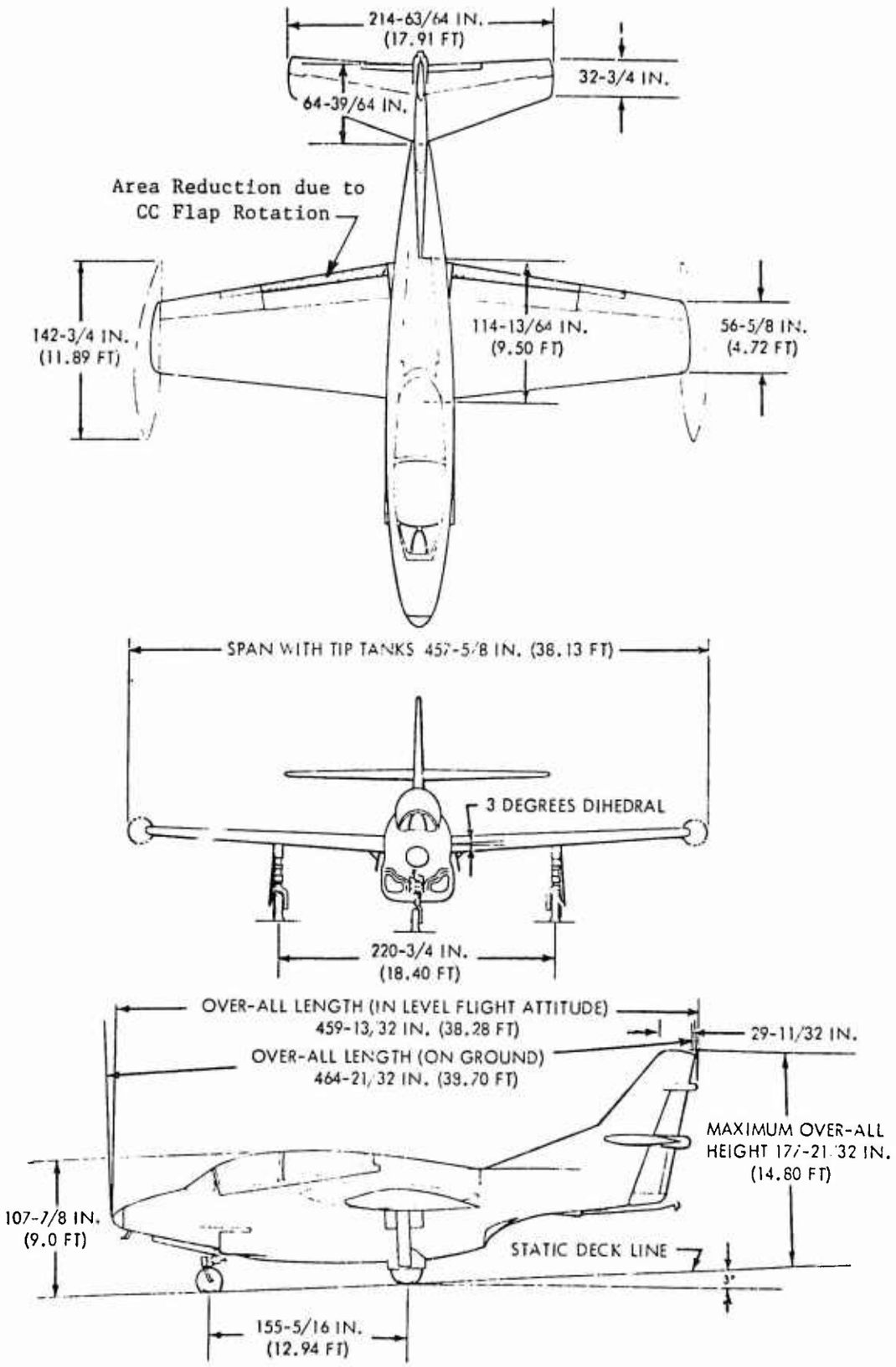

Figure 4 - Three View of T-2C Aircraft
(from NAVAIR 01-60GAB-2-1)

Values at M.A.C. (6.0" inboard of blown-unblown junction)

C = 17.76"	r/C = 0.0364	$X/C\|_{slot}$ = 0.850
C_l = 15.74"	r/C_l = 0.0411	$X/C_l\|_{slot}$ = 0.960
h = .020"	h/r = 0.0306	
r = .647"	t/C_l = 0.1354	
C_f = 2.66"		

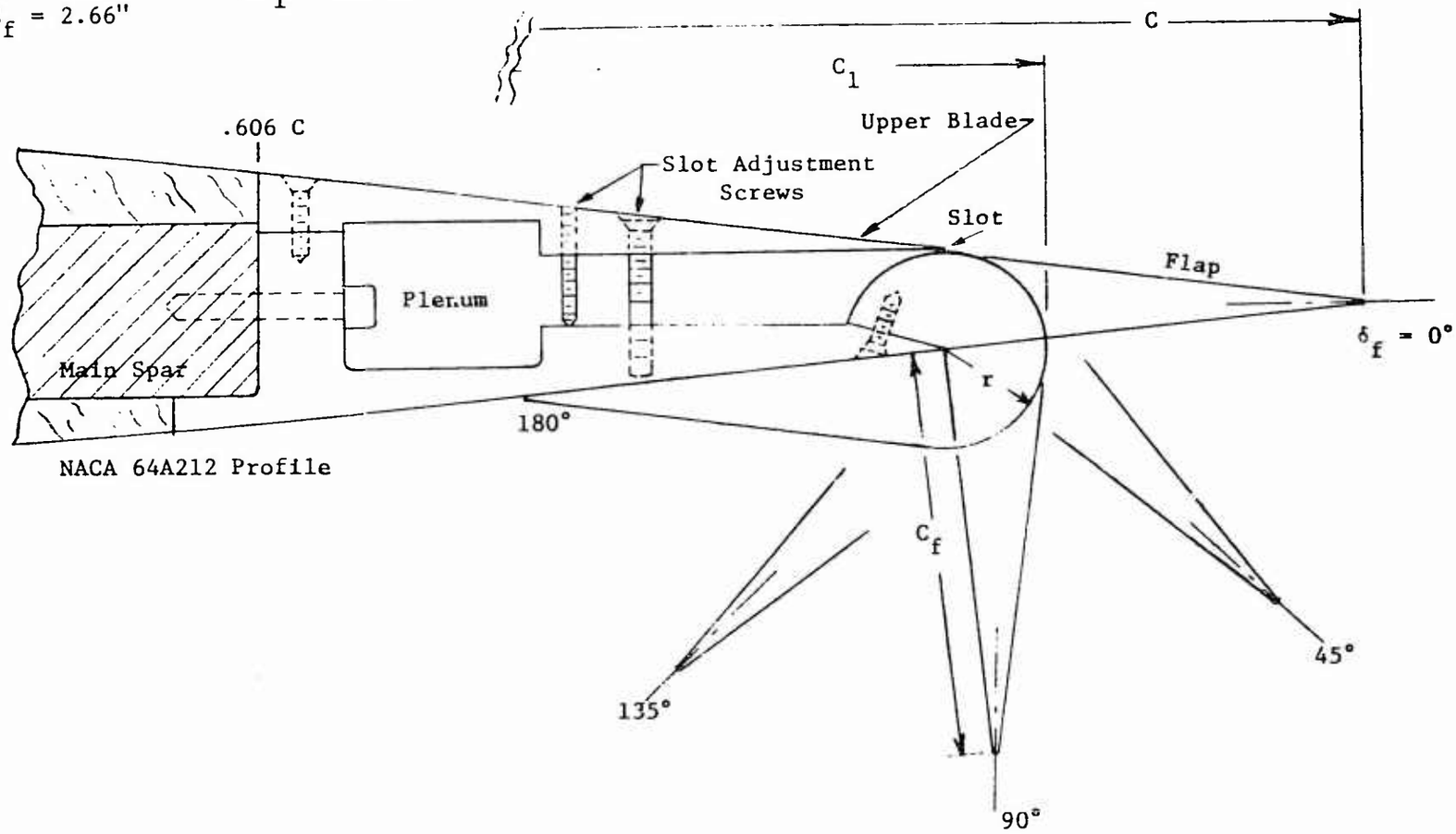

Figure 5 - Circulation Control Wing Trailing Edge Geometry

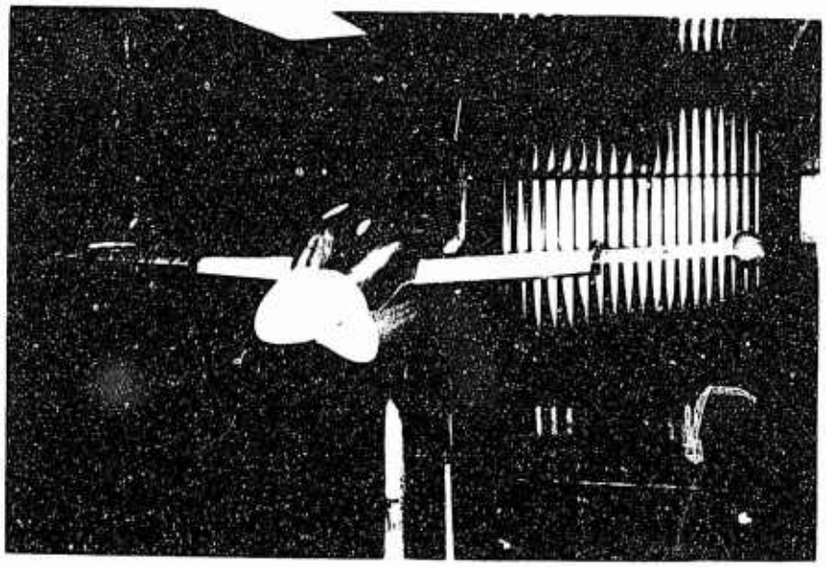

Front View Showing Inlet Fairings and Leading Edge Droop

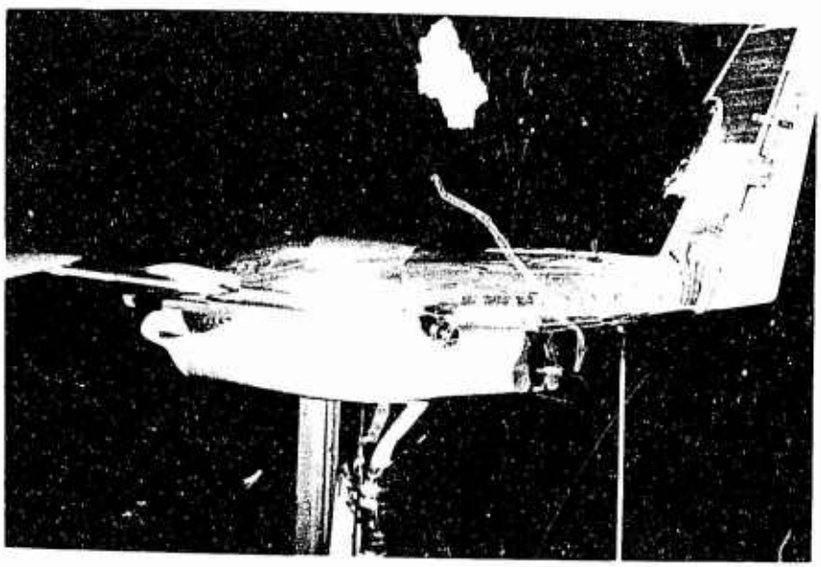

Side View Showing Air Supply Connections

Figure 6 - Model Installation in NSRDC 8 x 10-Foot Subsonic Tunnel

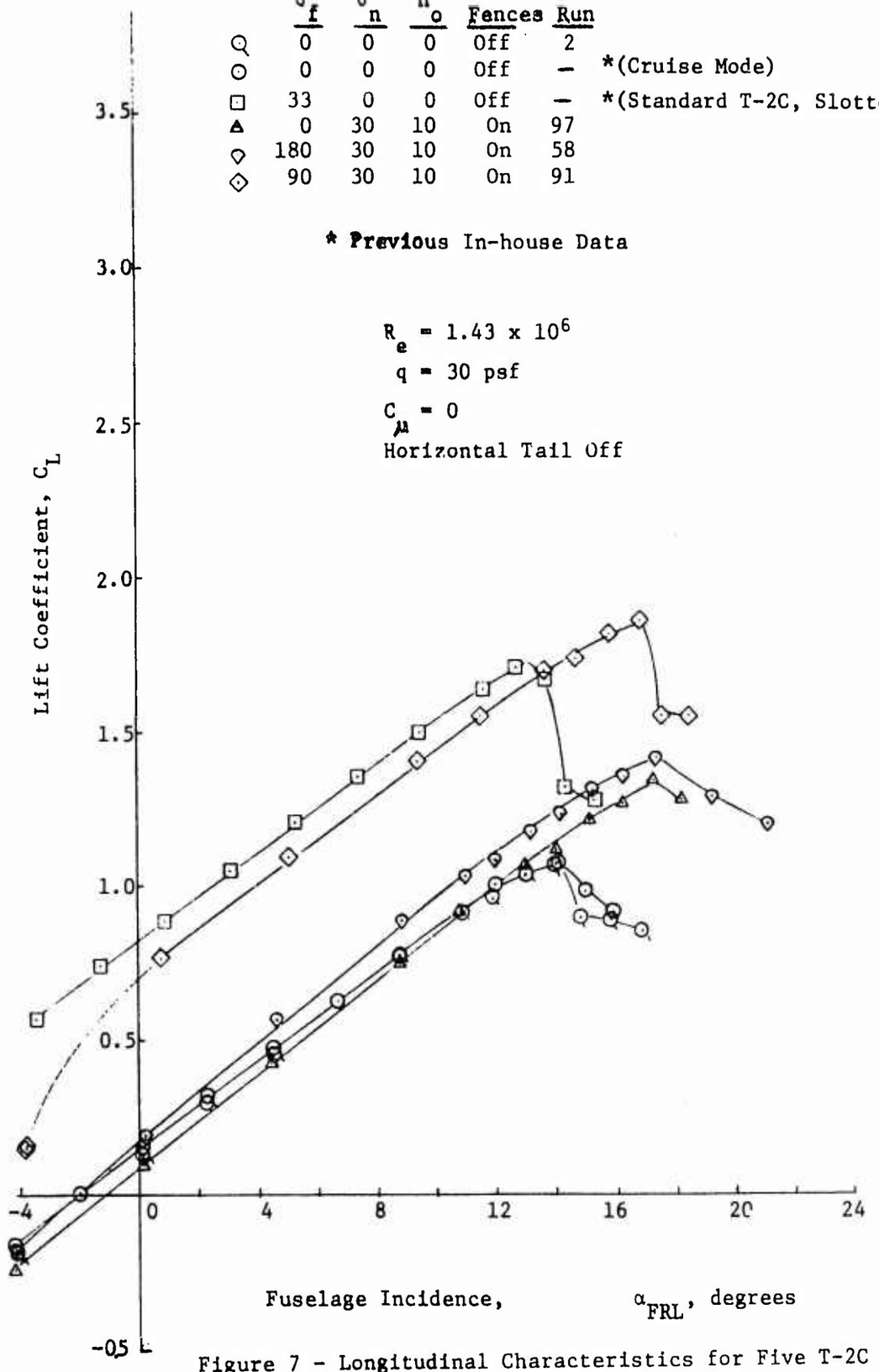

Figure 7 - Longitudinal Characteristics for Five T-2C Configurations without Blowing, Tail-Off

a. Lift Coefficient

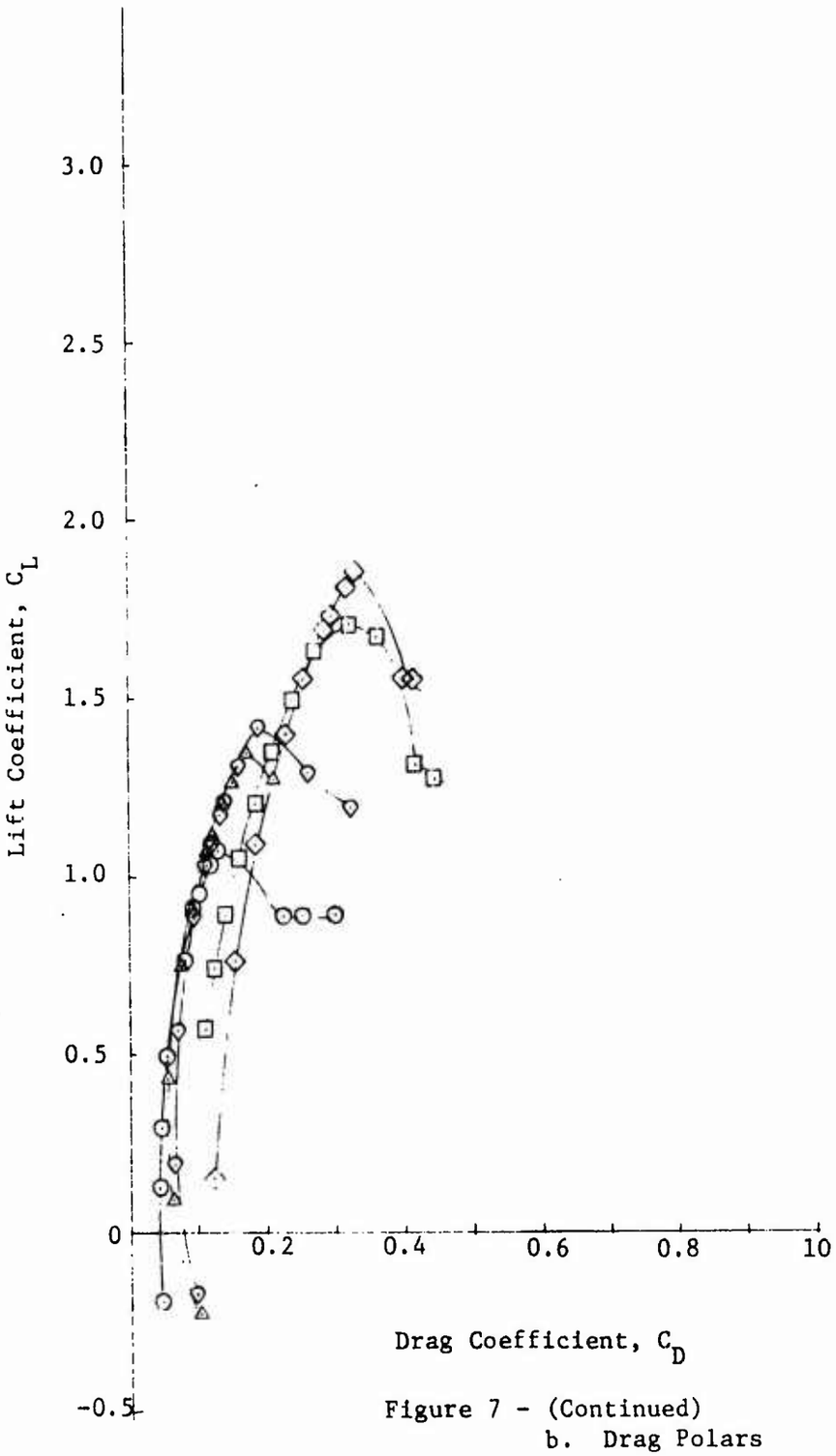

Figure 7 - (Continued)
b. Drag Polars

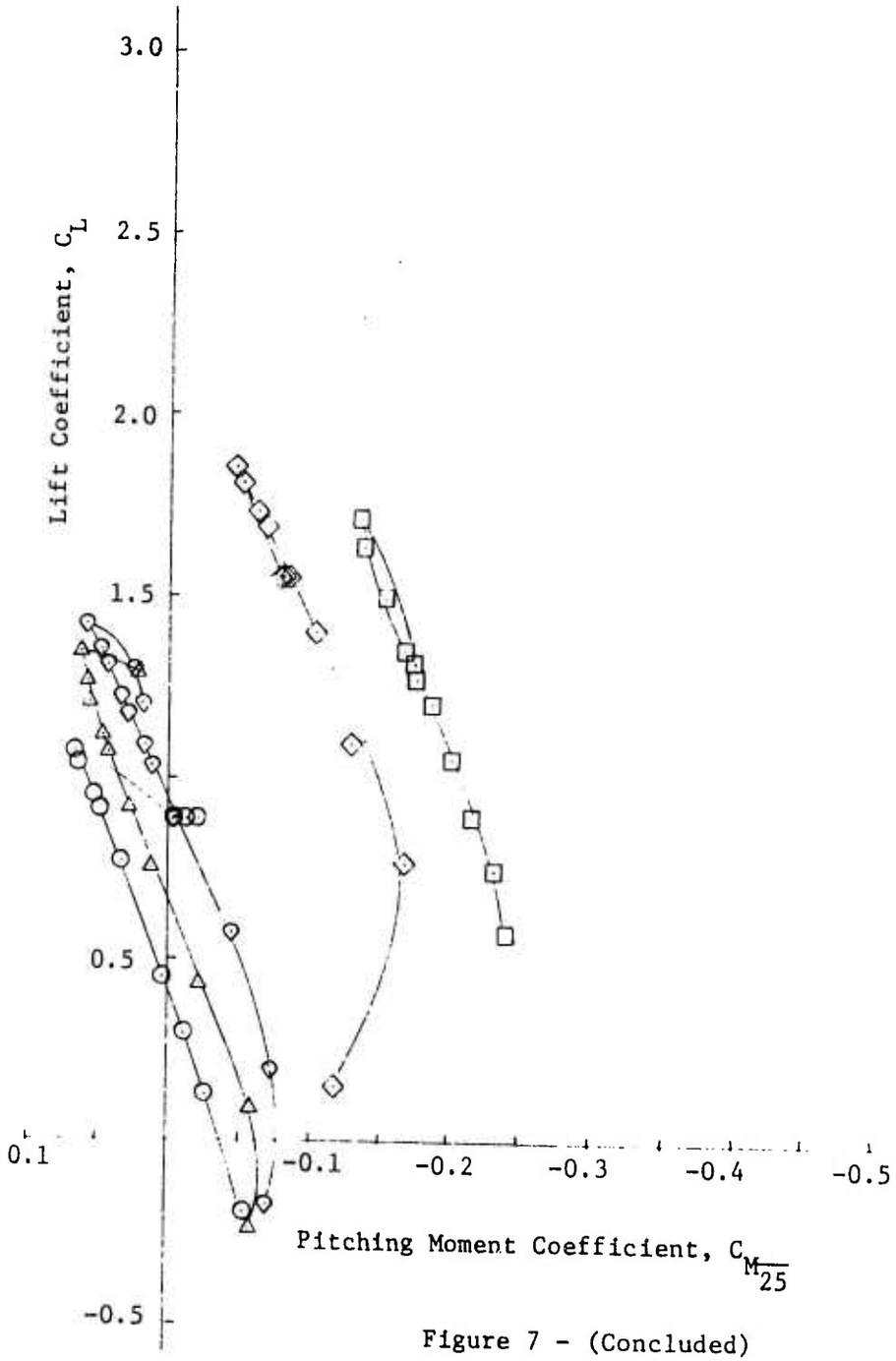

Figure 7 - (Concluded)
c. Pitching Moment

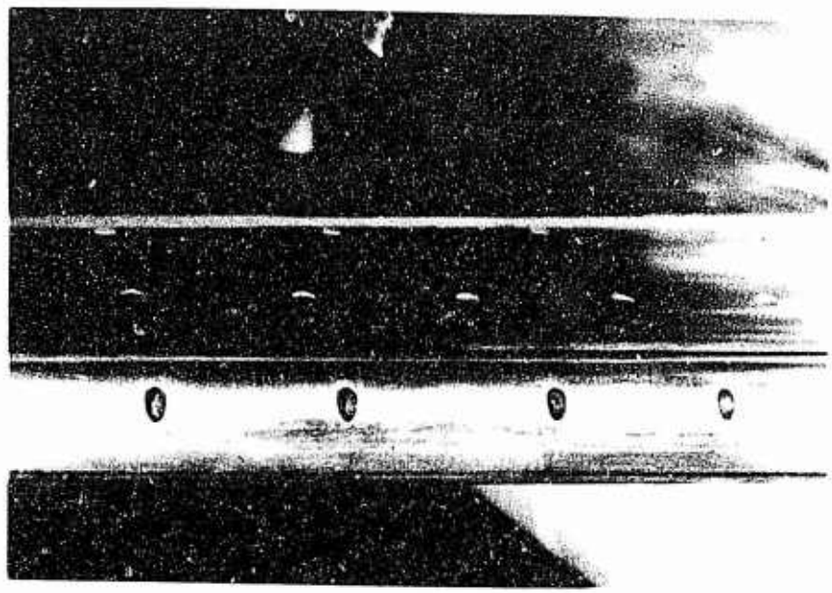

Slot, Trailing Edge, and Attachment Screws
(wax-filled)

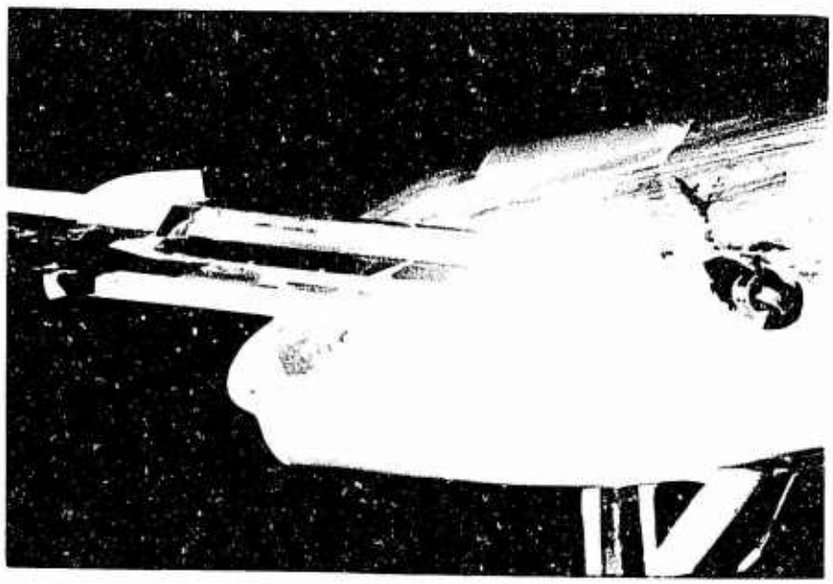

Cotton Tuft Showing Jet Turning ($q_\infty = 0$)

Figure 8 - Coanda Trailing Edge Detail and Jet Static Turning

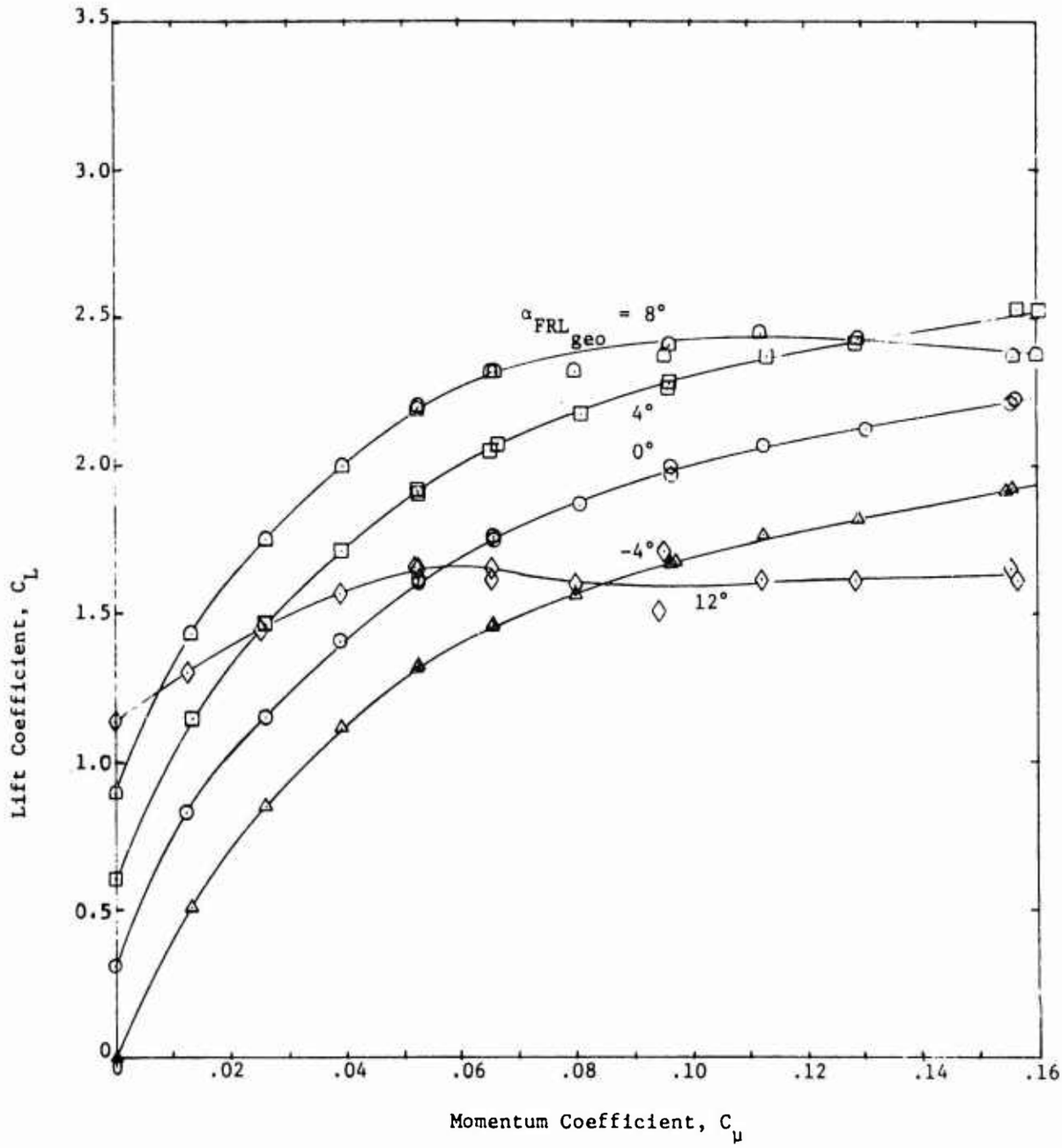

Figure 9 - Lift as a Function of Blowing for Configuration 2
(δ_f = 180°, δ_n = δ_{n_o} = 0°, No Fences)

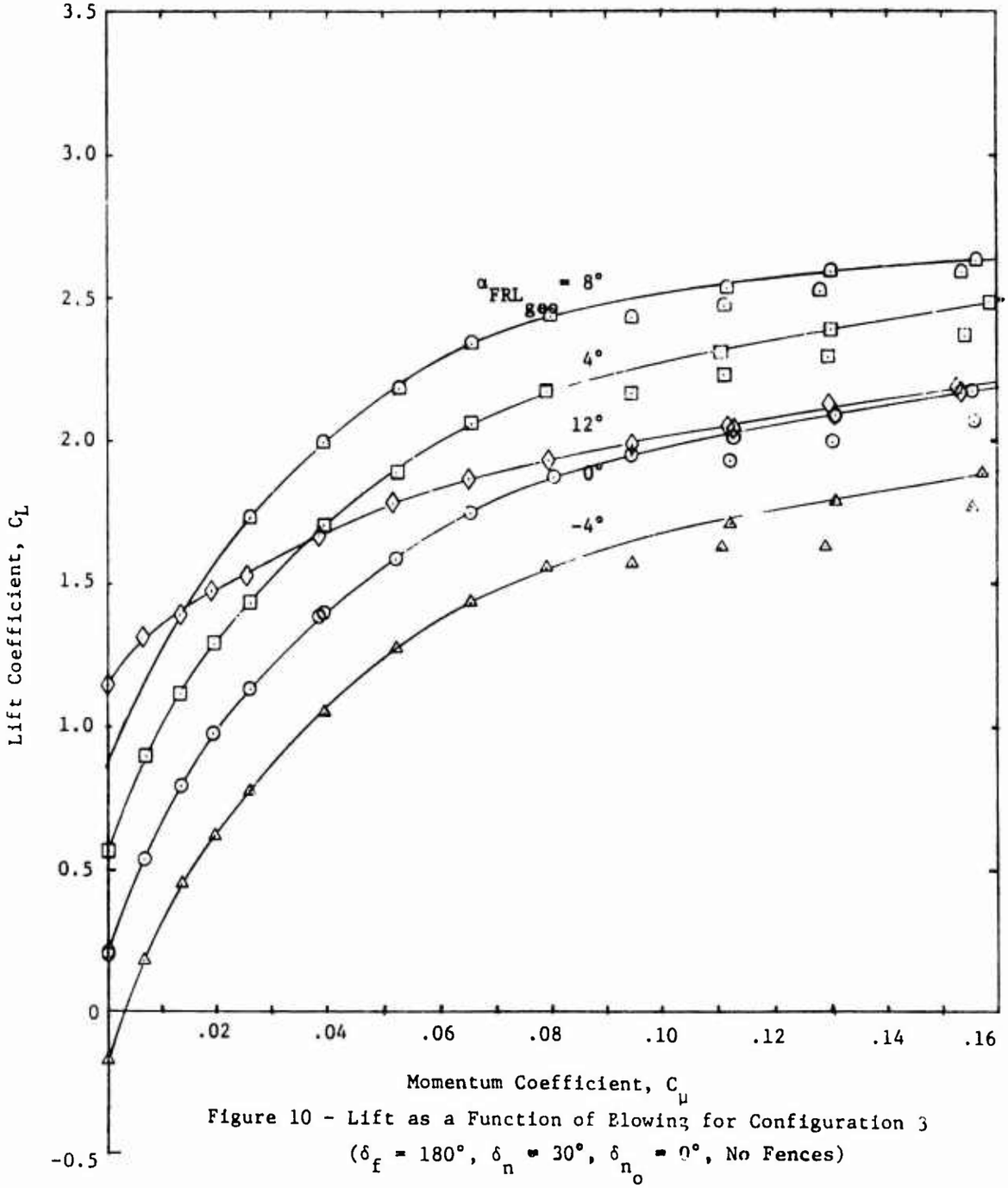

Figure 10 - Lift as a Function of Blowing for Configuration 3
(δ_f = 180°, δ_n = 30°, δ_{n_o} = 0°, No Fences)

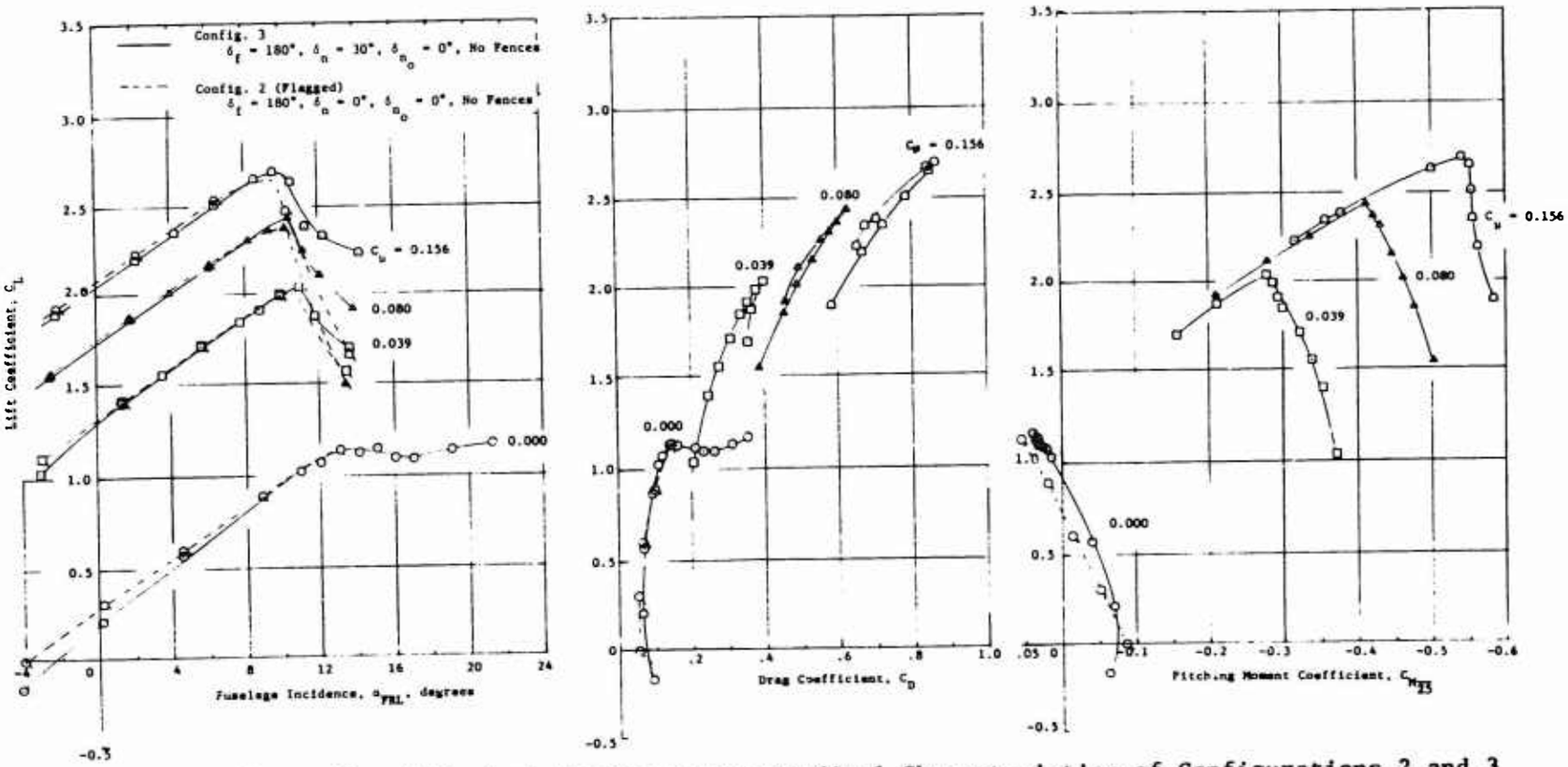

Figure 11 - Effect of Blowing on Longitudinal Characteristics of Configurations 2 and 3 (δ_{n_o} = 0°, No Fences)

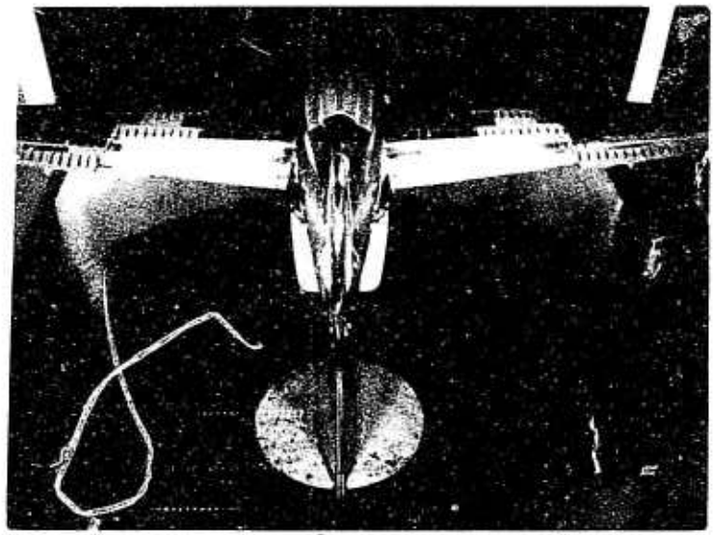

$\alpha_{FRL_{geo}} = 0°$ $P_d = 0$ in. Hg.

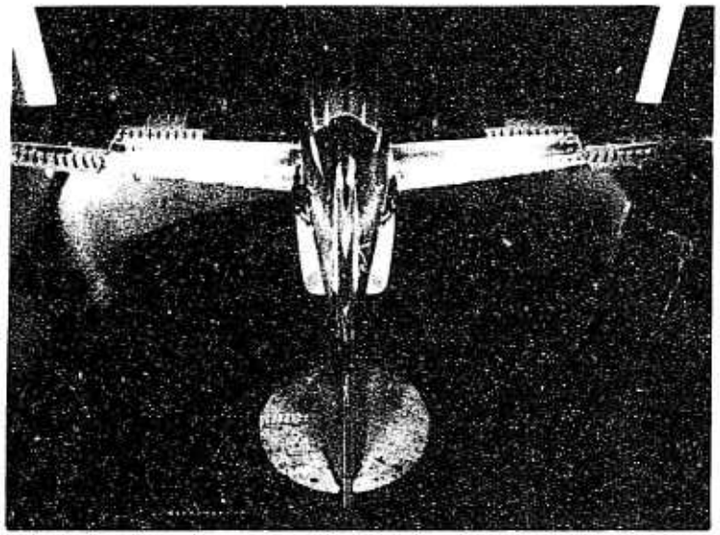

$\alpha_{FRL_{geo}} = 0°$ $P_d = 30$ in. Hg. ($C_\mu = 0.082$)

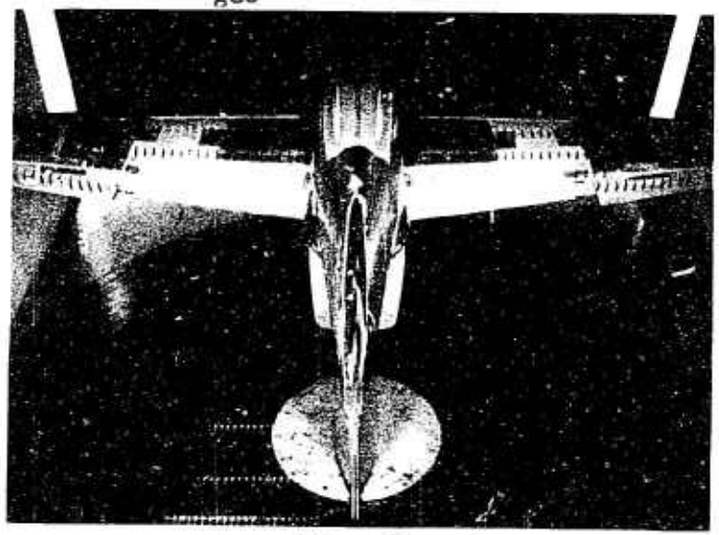

$\alpha_{FRL_{geo}} = 8°$ $P_d = 0$

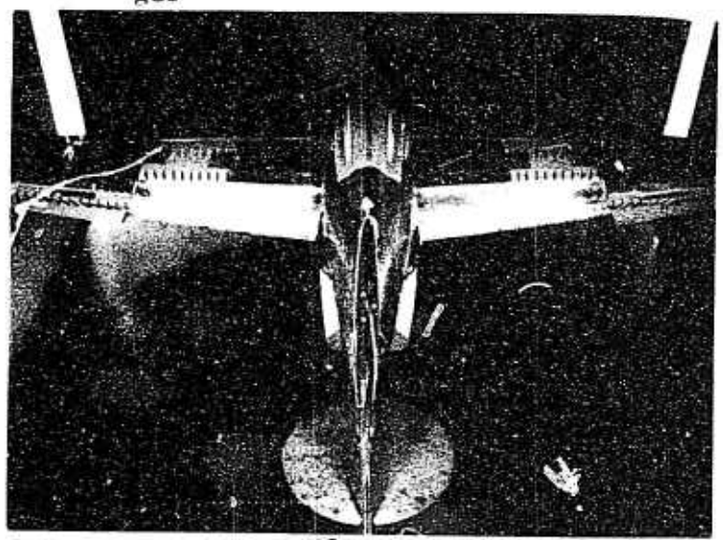

$\alpha_{FRL_{geo}} = 8°$ $P_d = 30$ in. Hg.

Figure 12 - Tuft Study of Flow Field with and without Blowing
(Config. 3: $\delta_f = 180°$, $\delta_n = 30°$, $\delta_{n_o} = 0°$, No Fences, $q_\infty = 30$ psf)

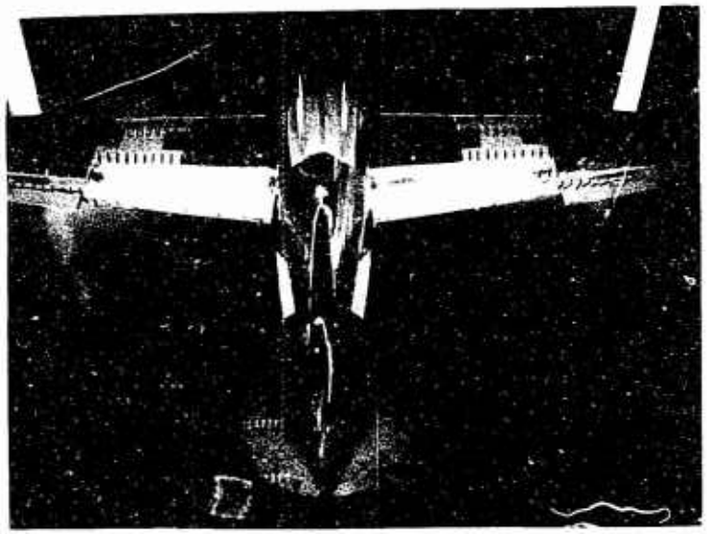

$\alpha_{FRL_{geo}}$ = 12° P_d = 0

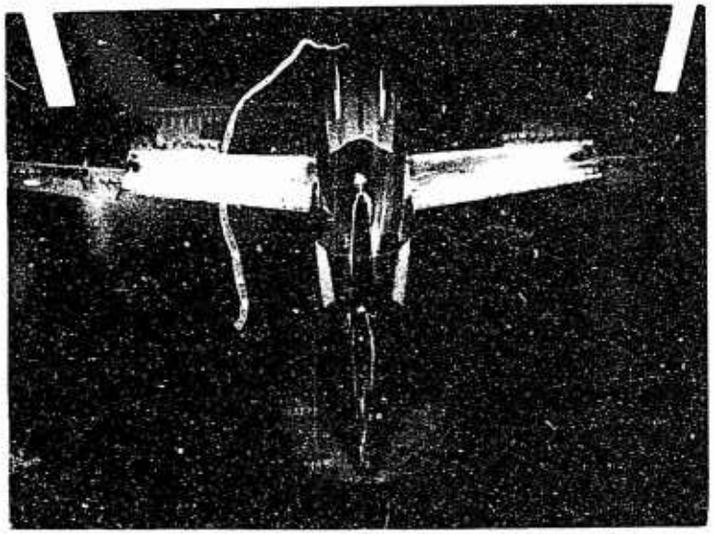

$\alpha_{FRL_{geo}}$ = 12° P_d = 30 in. Hg.

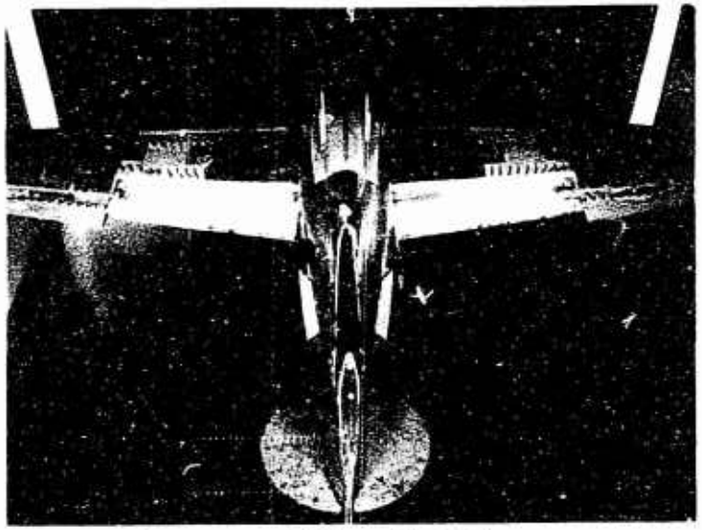

$\alpha_{FRL_{geo}}$ = 14° P_d = 0

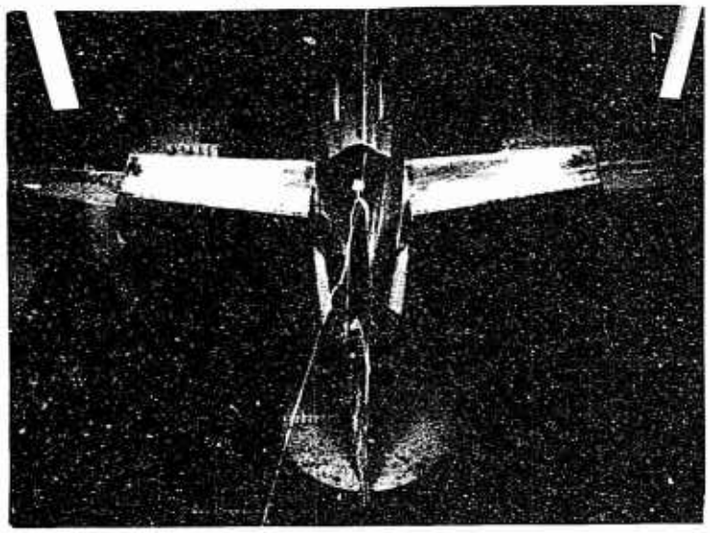

$\alpha_{FRL_{geo}}$ = 13° P_d = 30 in. Hg.

Figure 12 - (Concluded)

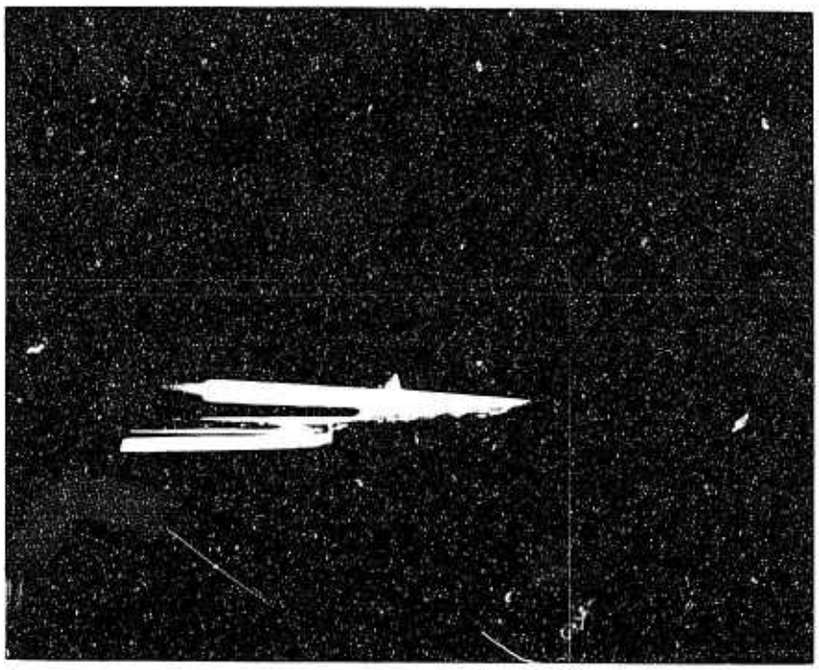

Right Wing, Looking Upstream from Below

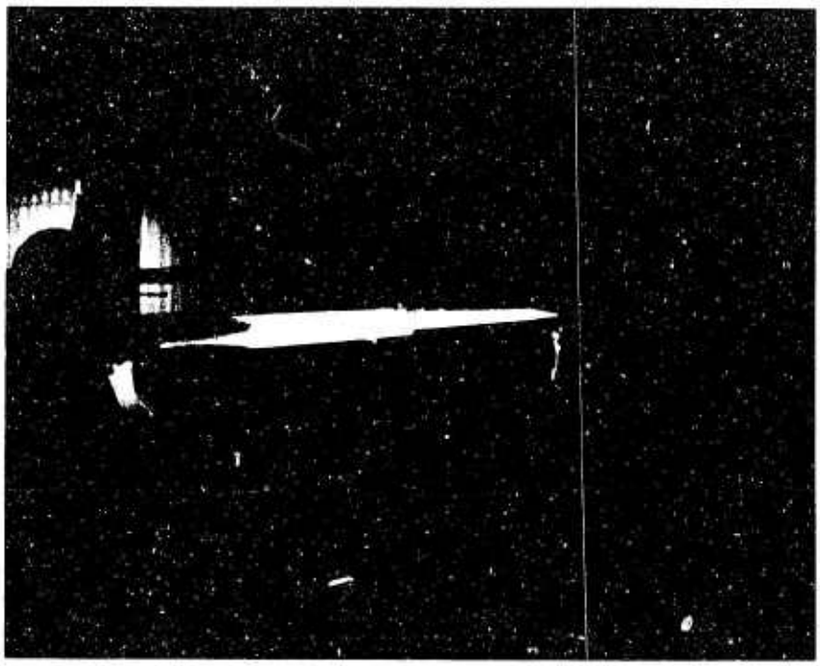

Right Wing, Looking Upstream from Slightly Above

Figure 13 - Helium Bubble Study of Mid-Span Vortex

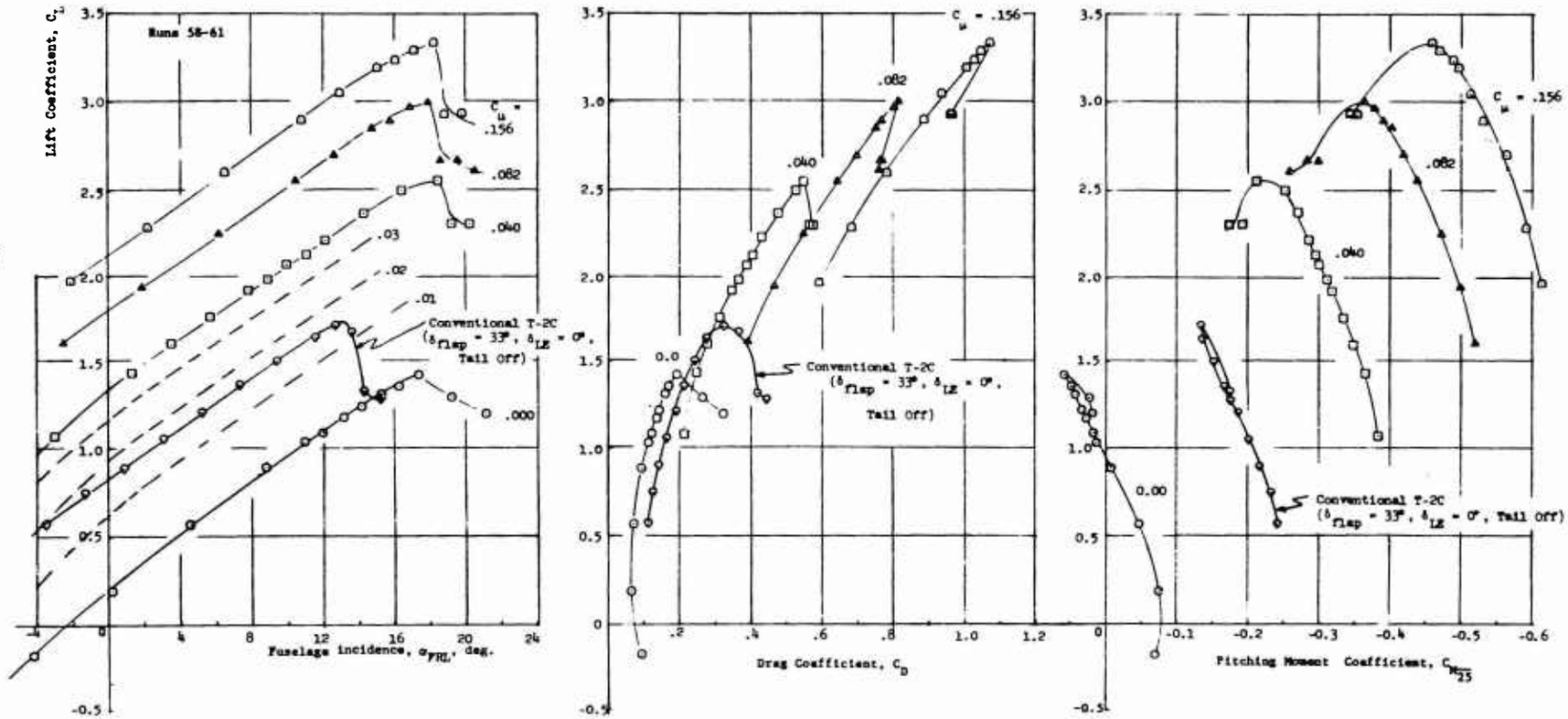

Figure 14 - Effect of Blowing on Longitudinal Characteristics of Configuration 4
(δ_f = 180°, δ_n = 30°, δ_{n_o} = 10°, Fences, Tail-Off)

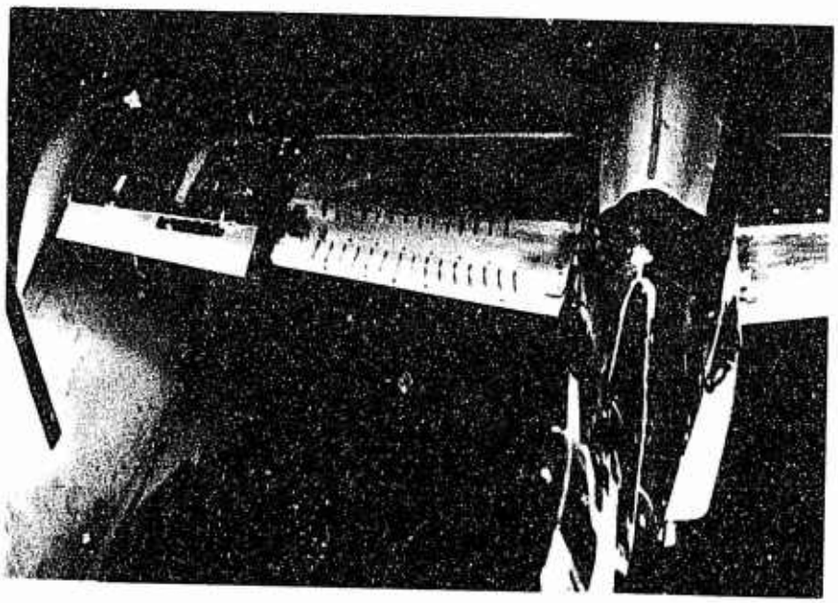

$\alpha_{FRL_{geo}} = 8°$

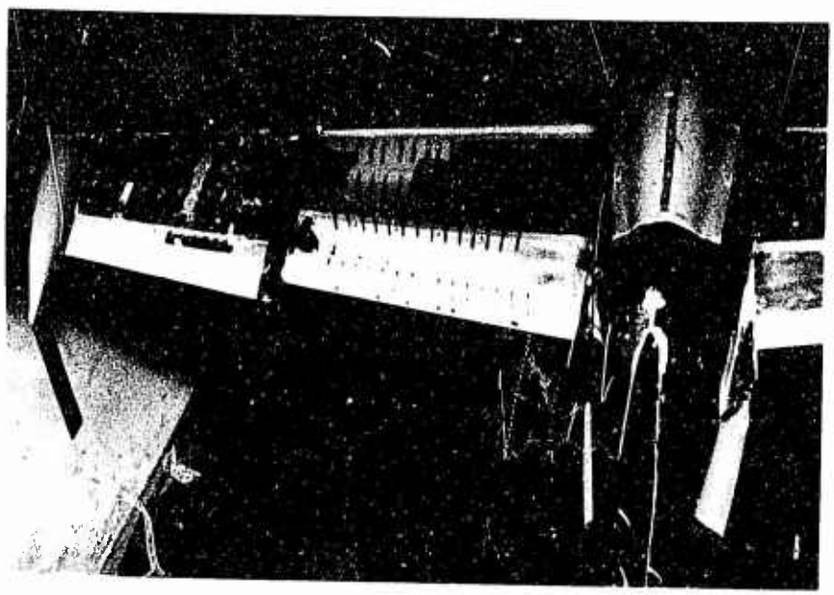

$\alpha_{FRL_{geo}} = 17.1°$

Figure 15 - Tuft Study of Flow Field with Fences Installed and Outboard Leading Edge Droop ($\delta_f = 180°$, $\delta_n = 30°$, $\delta_{n_o} = 10°$, Fences, $q_\infty = 20$ psf, $P_d = 25$ in. Hg., $C_\mu = .099$)

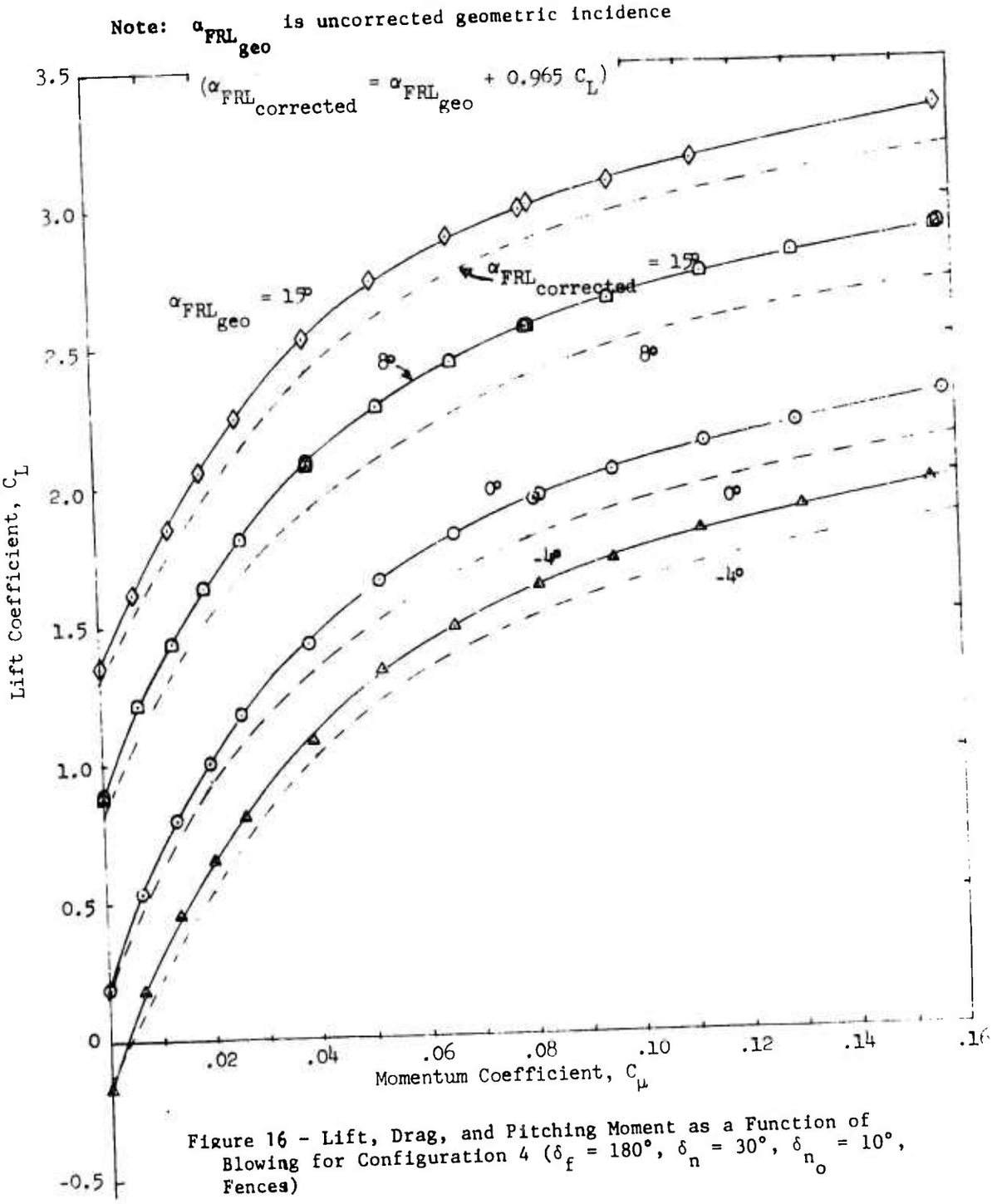

Figure 16 - Lift, Drag, and Pitching Moment as a Function of Blowing for Configuration 4 ($\delta_f = 180°$, $\delta_n = 30°$, $\delta_{n_o} = 10°$, Fences)

a. Lift Coefficient

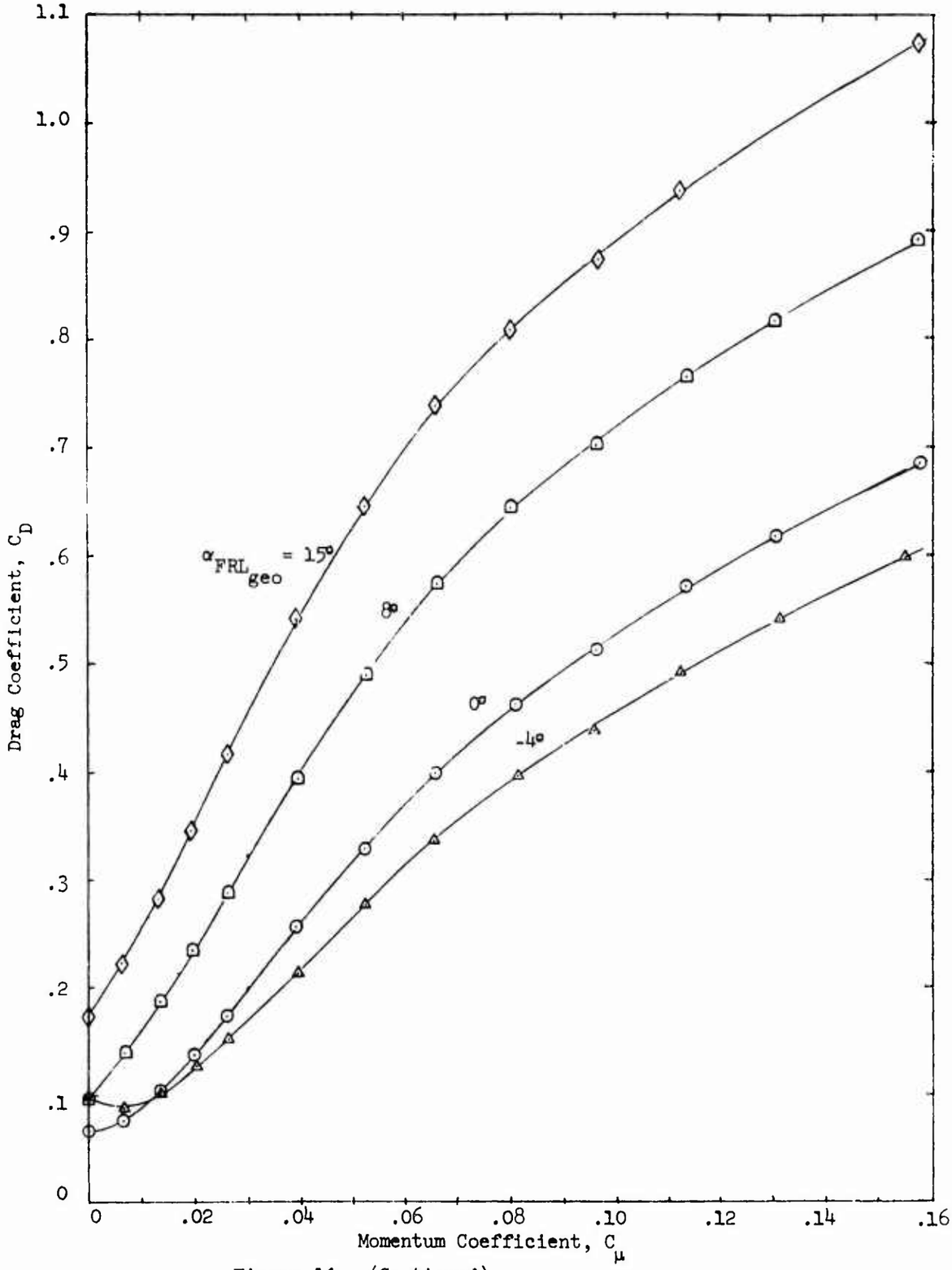

Figure 16 - (Continued)
b. Drag Coefficient

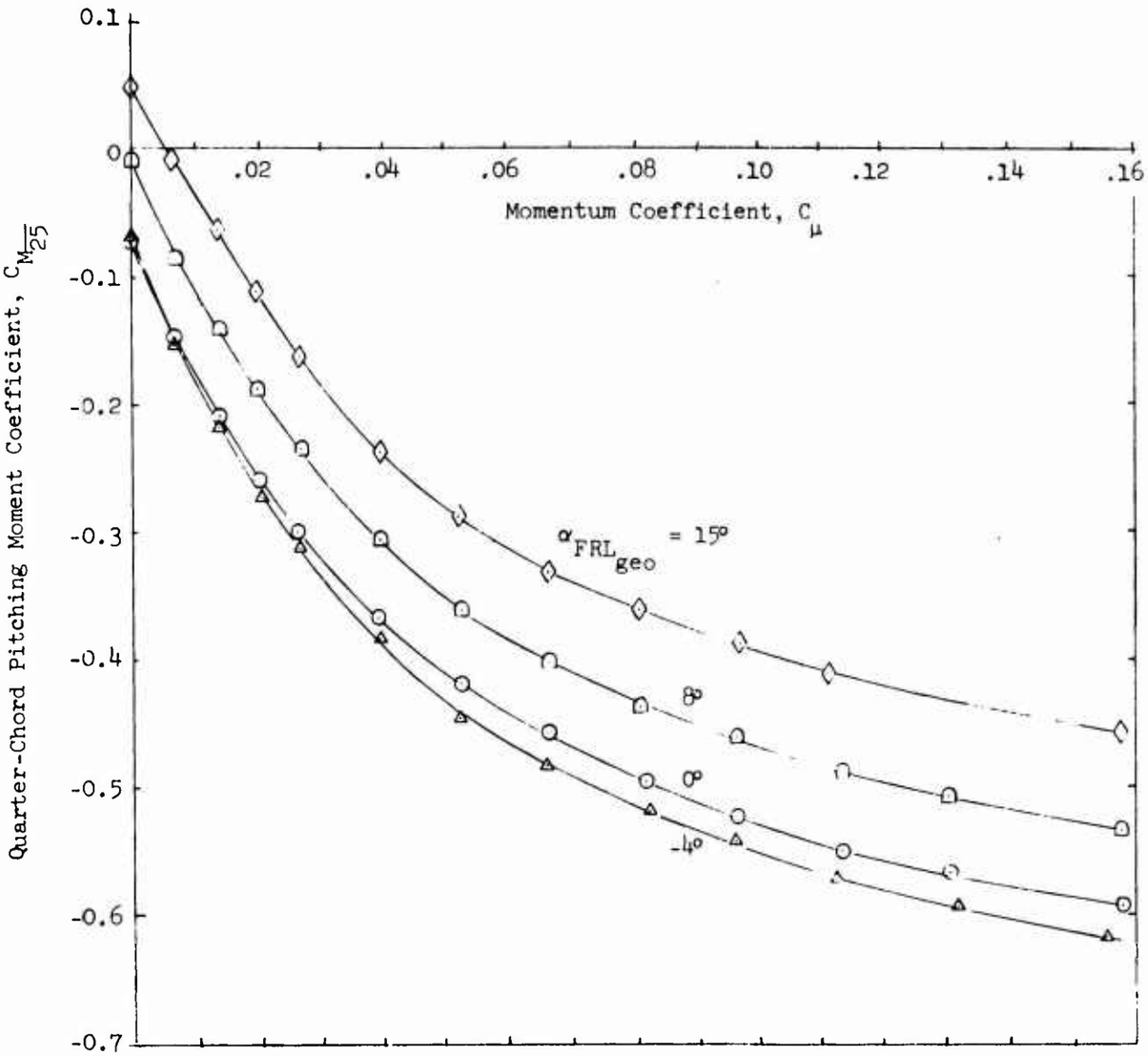

Figure 16 - (Concluded)
c. Mean Quarter-Chord Pitching Moment Coefficient

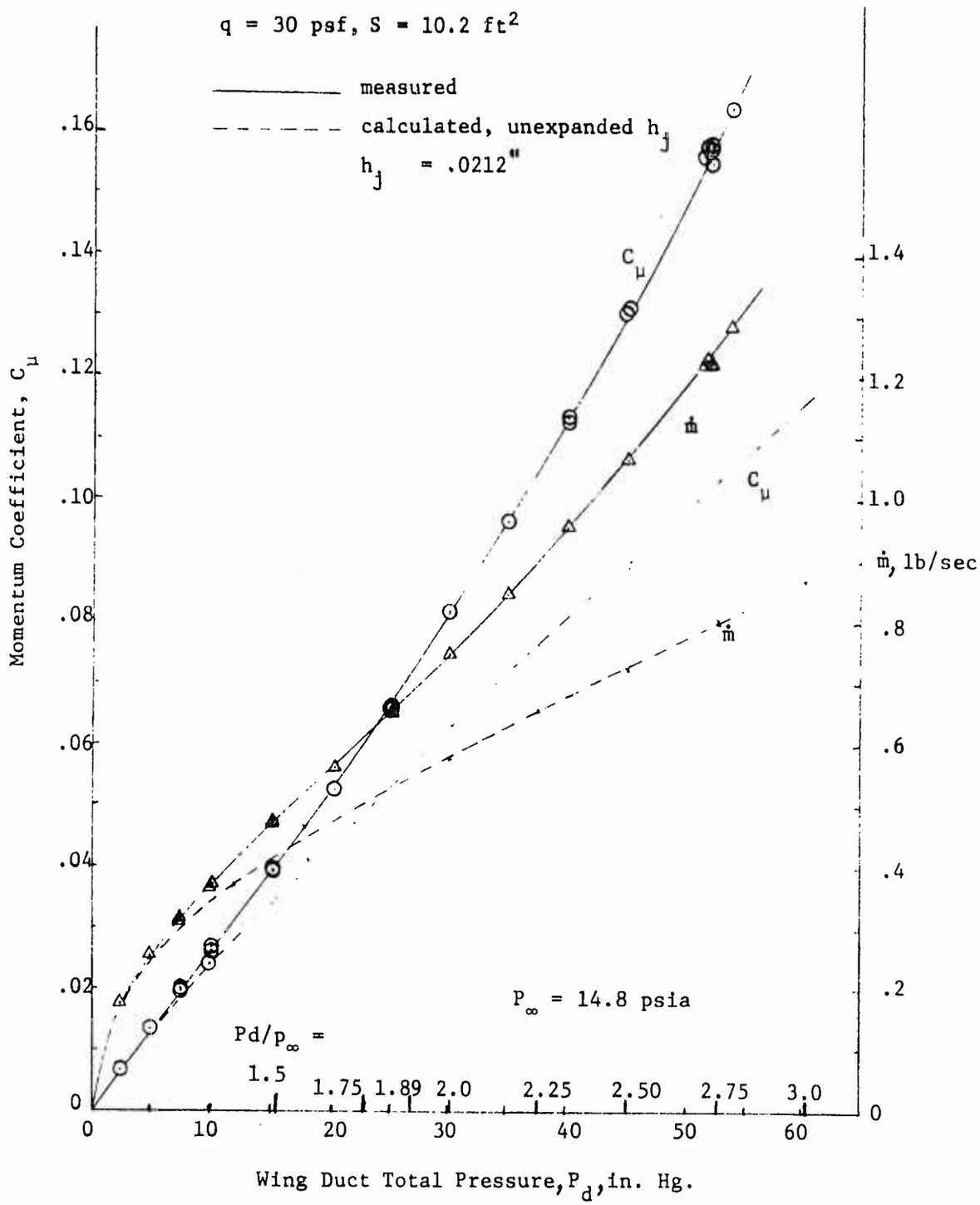

Figure 17 - Measured and Calculated Momentum Coefficient as a Function of Wing Duct Total Pressure

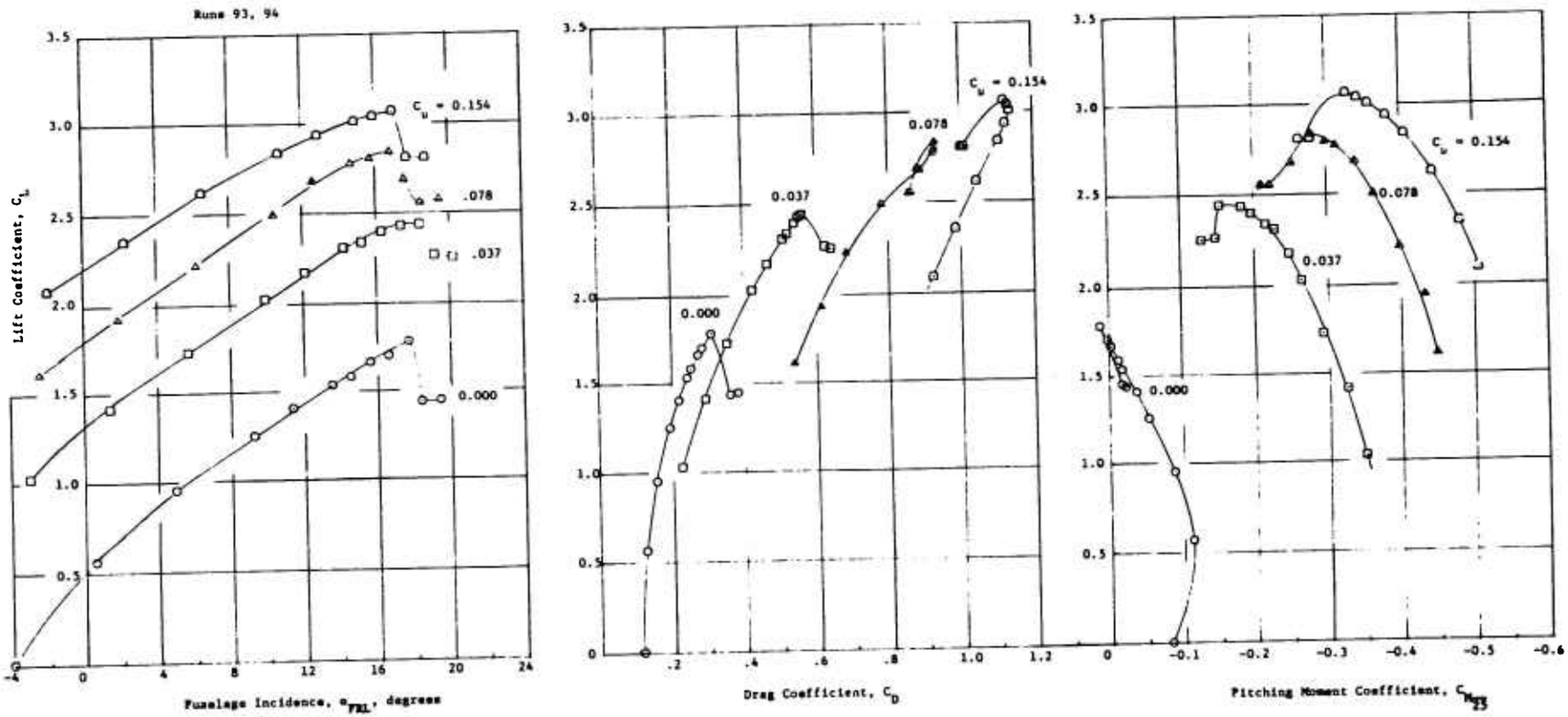

Figure 18 - Effect of Blowing on Longitudinal Characteristics of Configuration 8
(δ_f = 135°, δ_n = 30°, δ_{n_o} = 10°, Fences, Tail-Off)

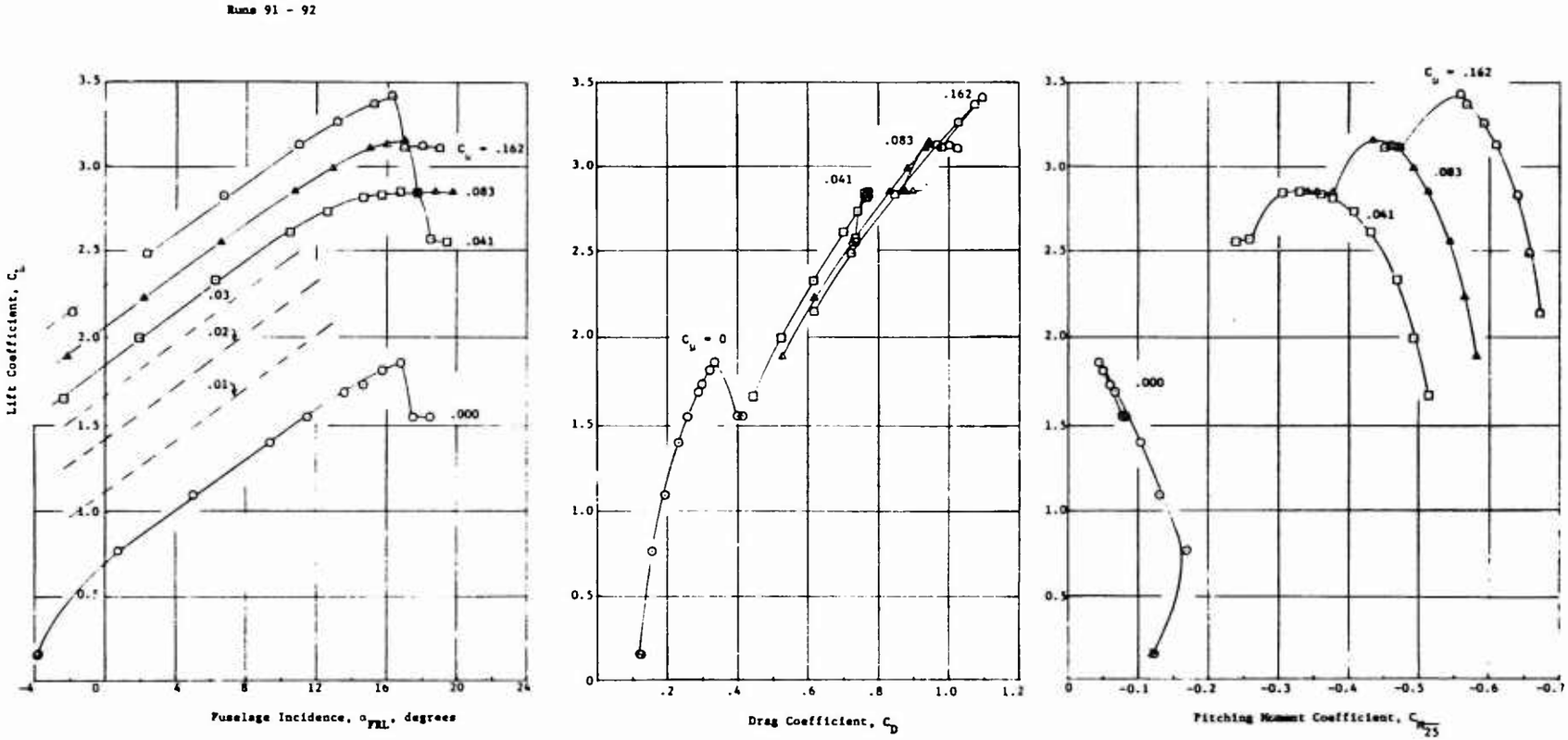

Figure 19 - Effect of Blowing on Longitudinal Characteristics of Configuration 7 (δ_f = 90°, δ_n = 30°, δ_{n_o} = 10°, Fences, Tail-Off)

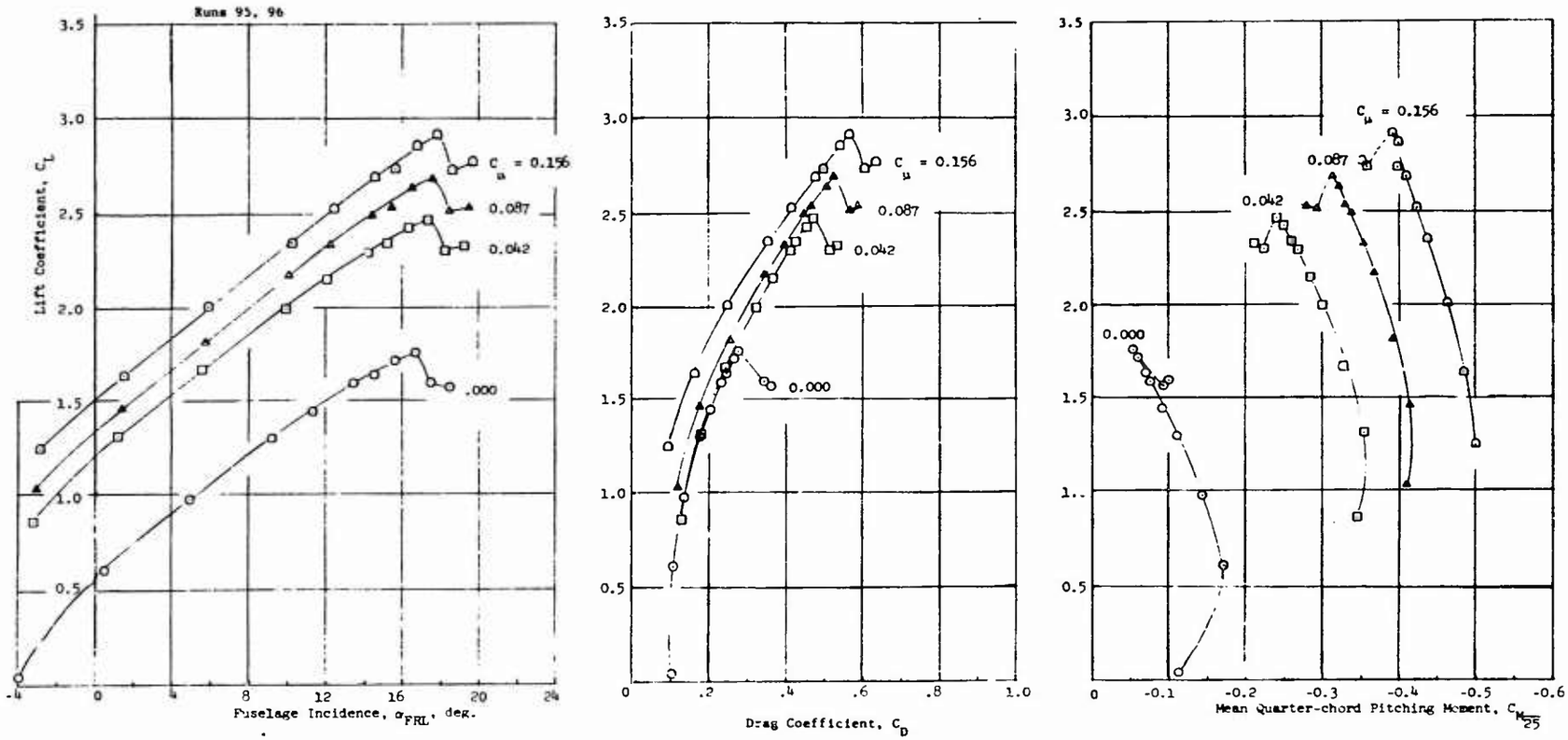

Figure 20 - Effect of Blowing on Longitudinal Characteristics of Configuration 9 (δ_f = 45°, δ_n = 30°, δ_{n_o} = 10°, Fences, Tail-off)

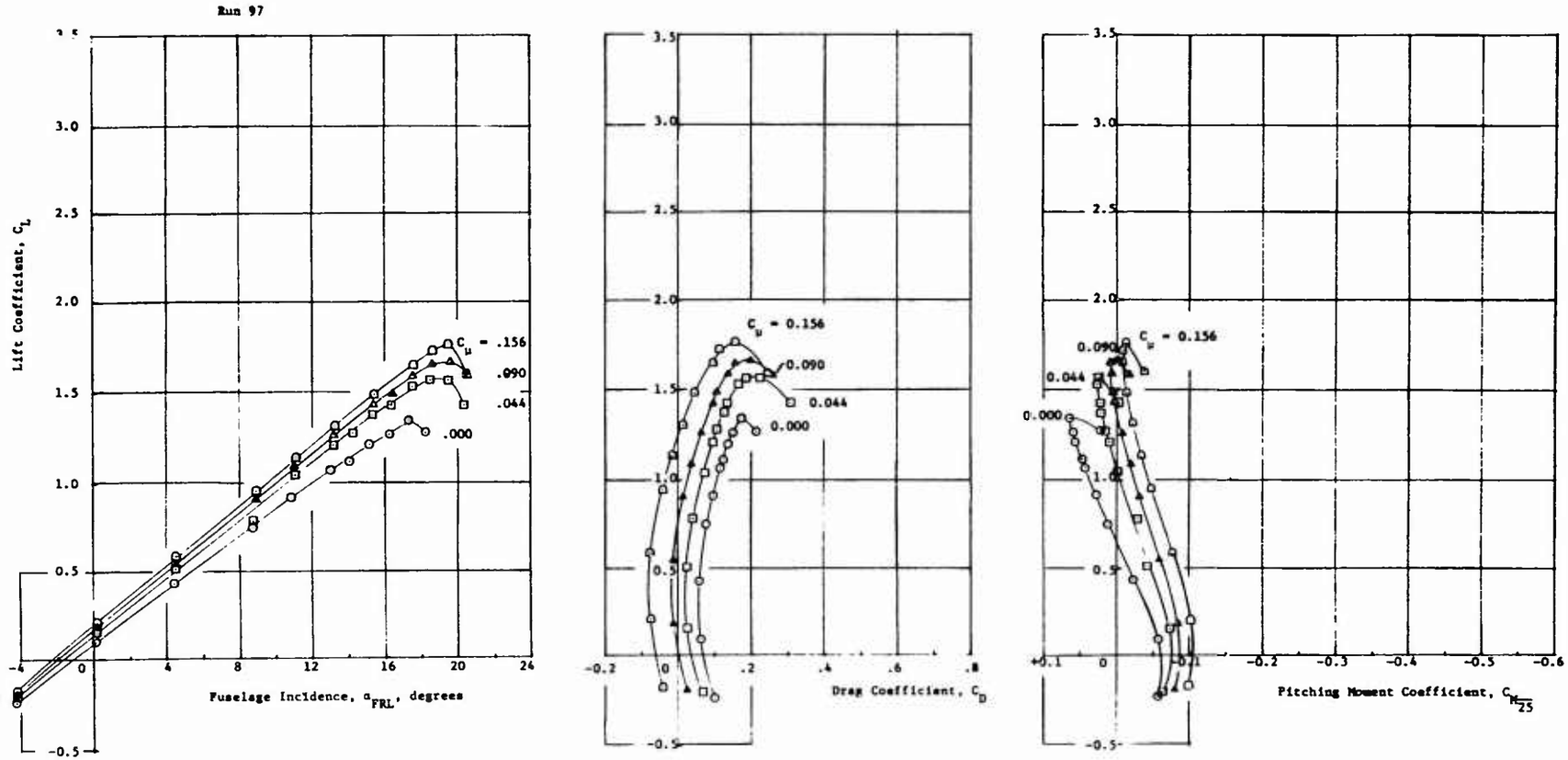

Figure 21 - Effect of Blowing on Longitudinal Characteristics of Configuration 10 (δ_f = 0°, δ_n = 30°, δ_{n_o} = 10°, Fences, Tail-Off)

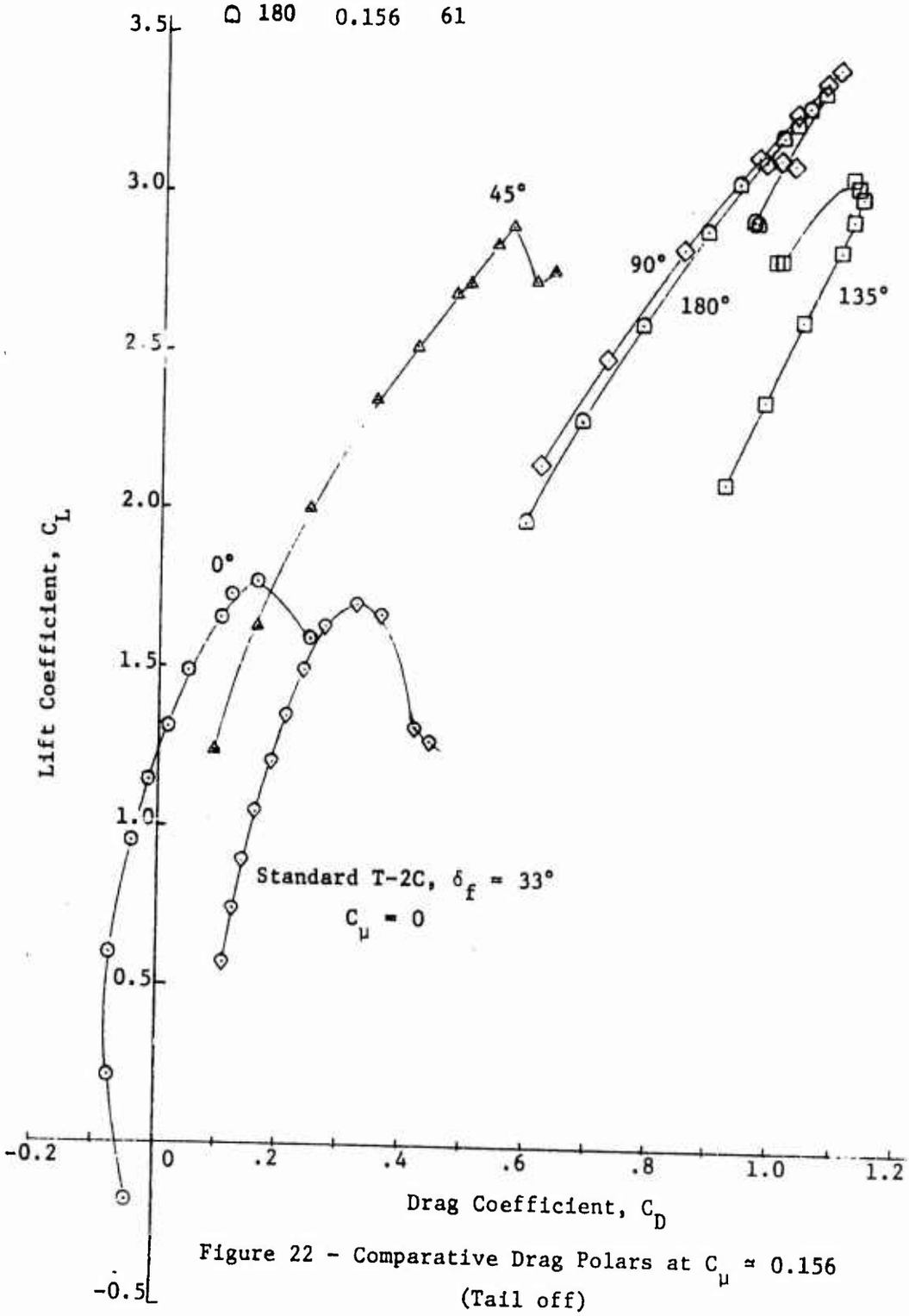

Figure 22 - Comparative Drag Polars at $C_\mu \approx 0.156$
(Tail off)

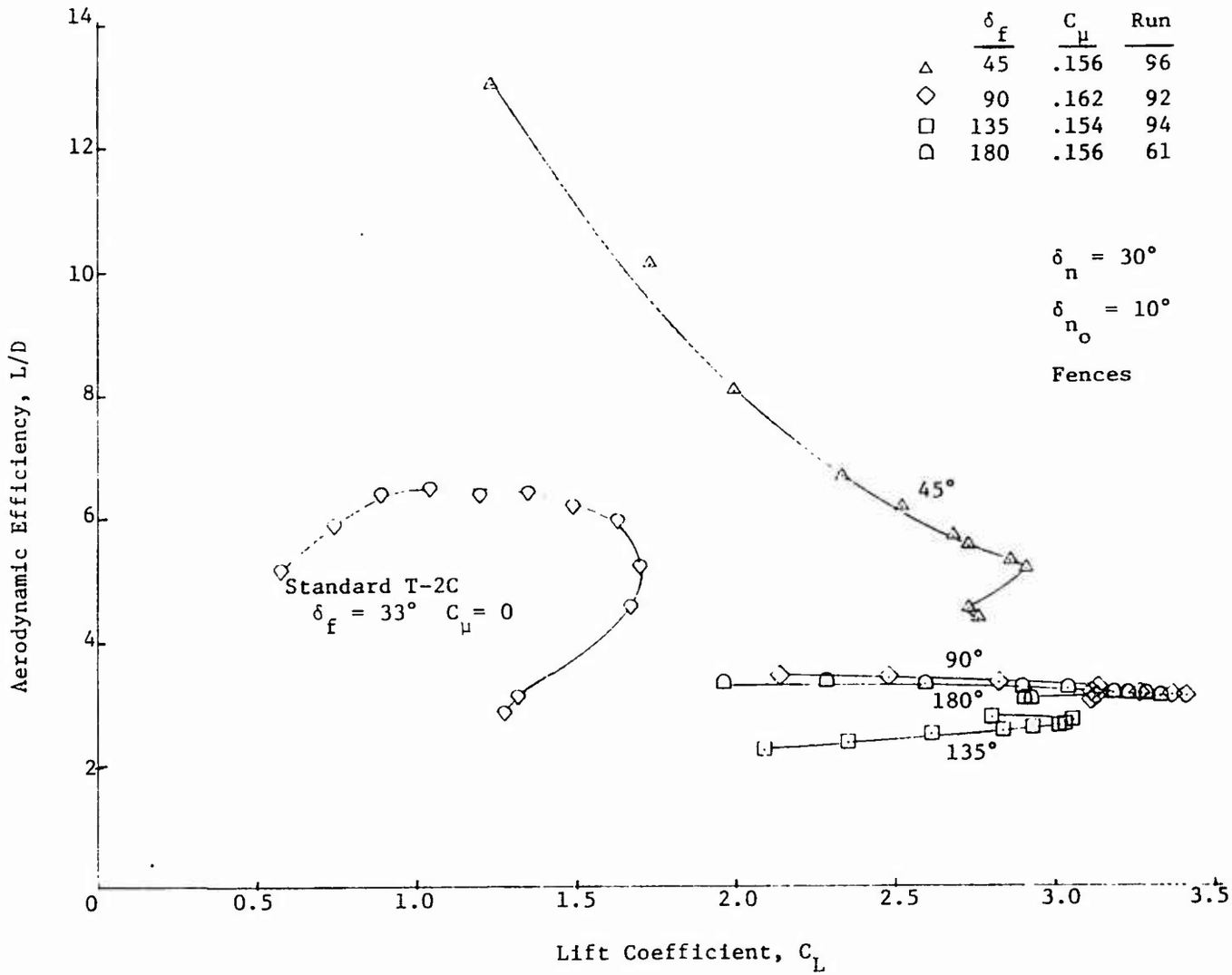

Figure 23 - Comparative Efficiencies at $C_\mu \simeq 0.156$ (Tail Off)

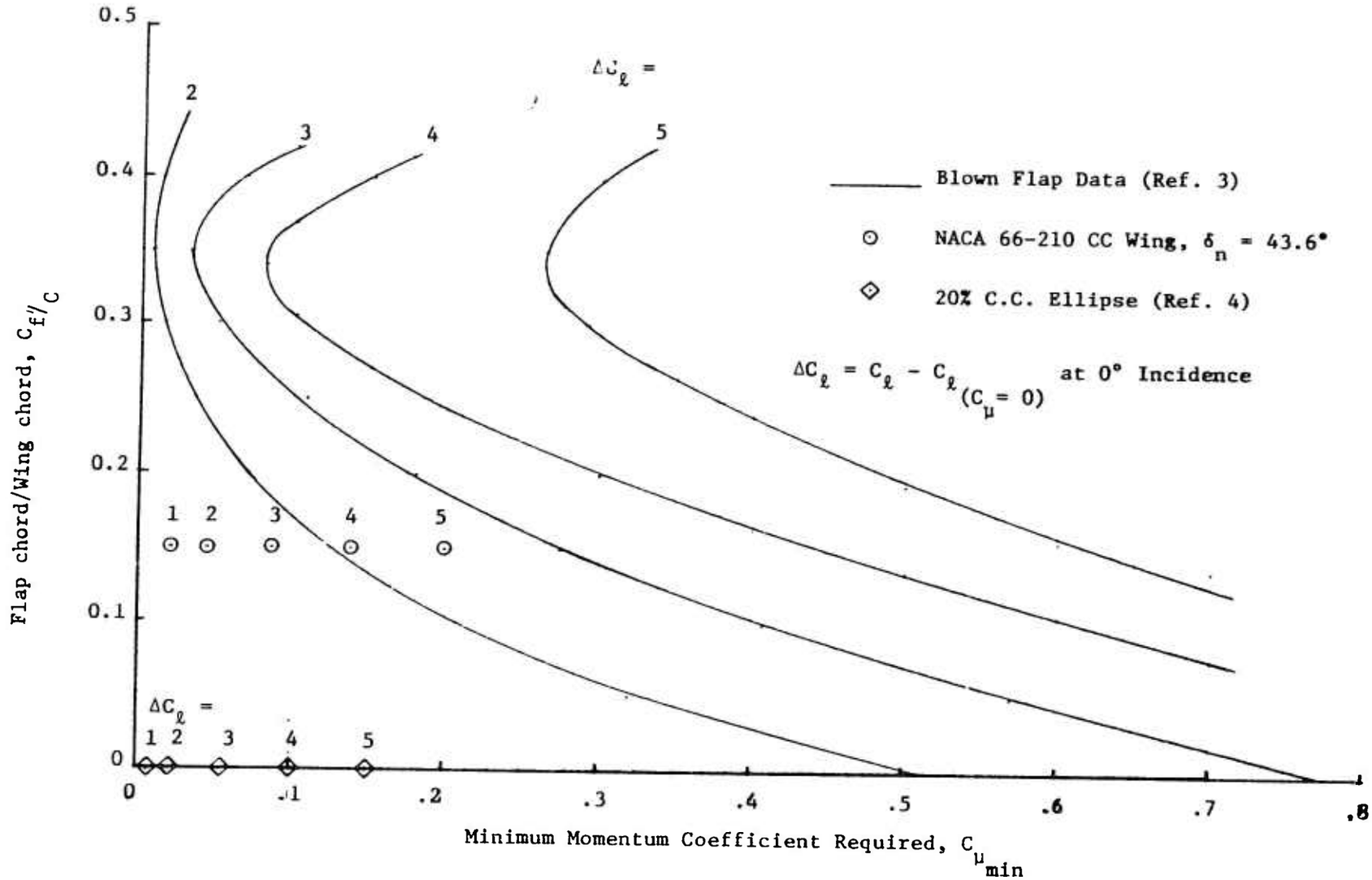

Figure 24 - Comparison of Two-Dimensional Lift Data for Blown Flaps and Circulation Control Airfoils at $\alpha = 0°$

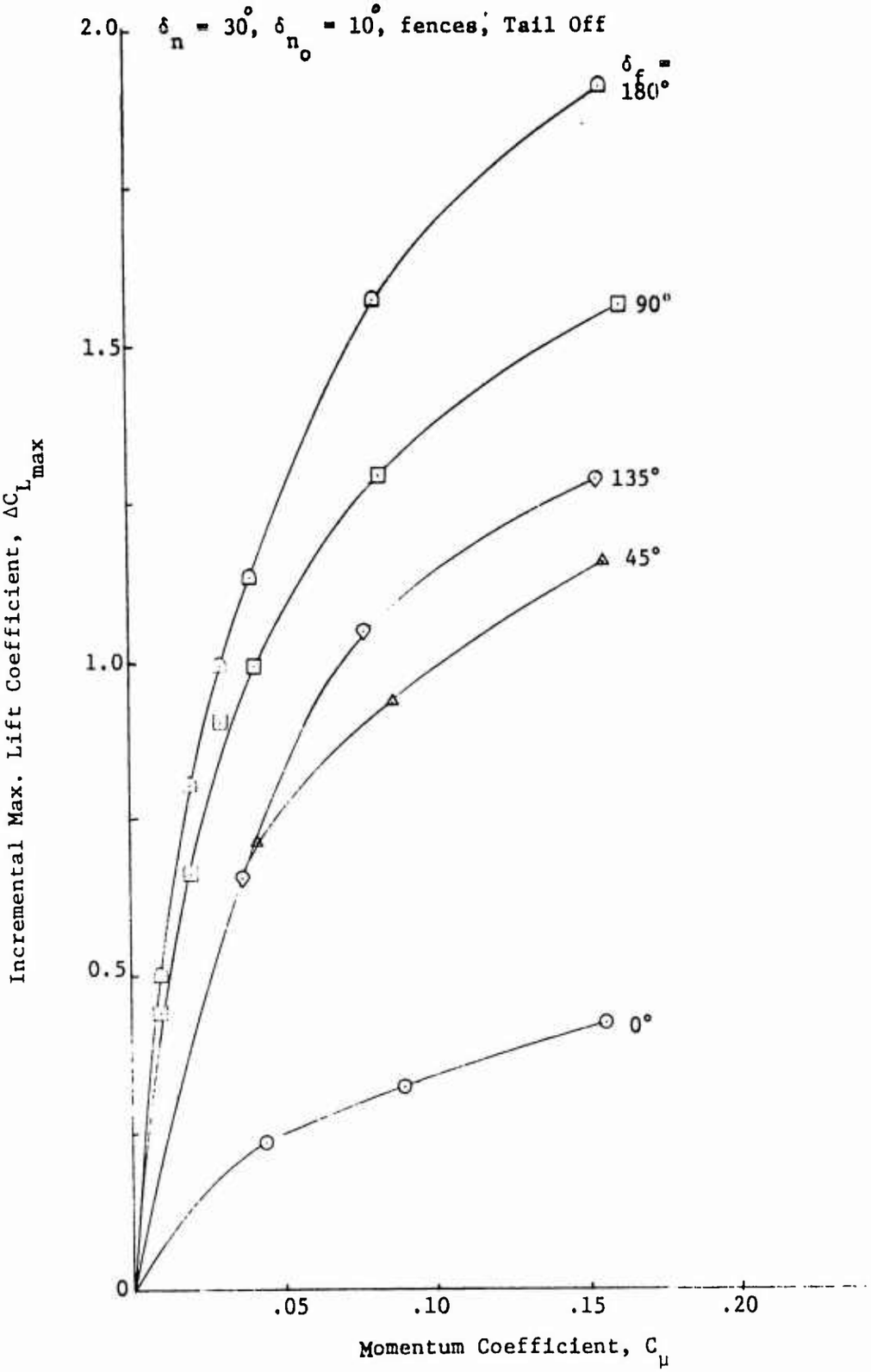

Figure 25 - Incremental $C_{L_{max}}$ due to Blowing for Five Flap Deflection Angles

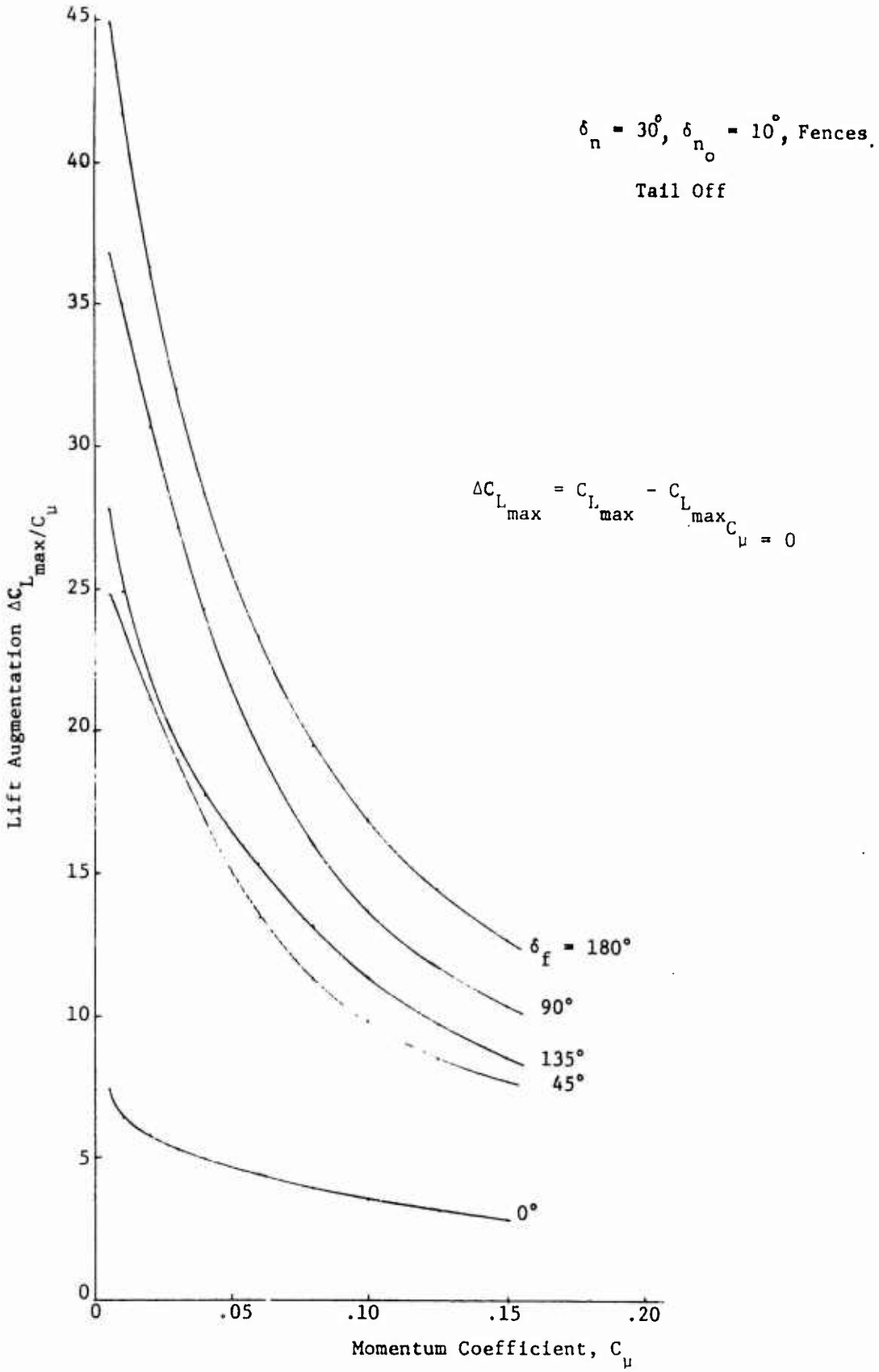

Figure 26 - Lift Augmentation due to Blowing for Flap Deflection Angles

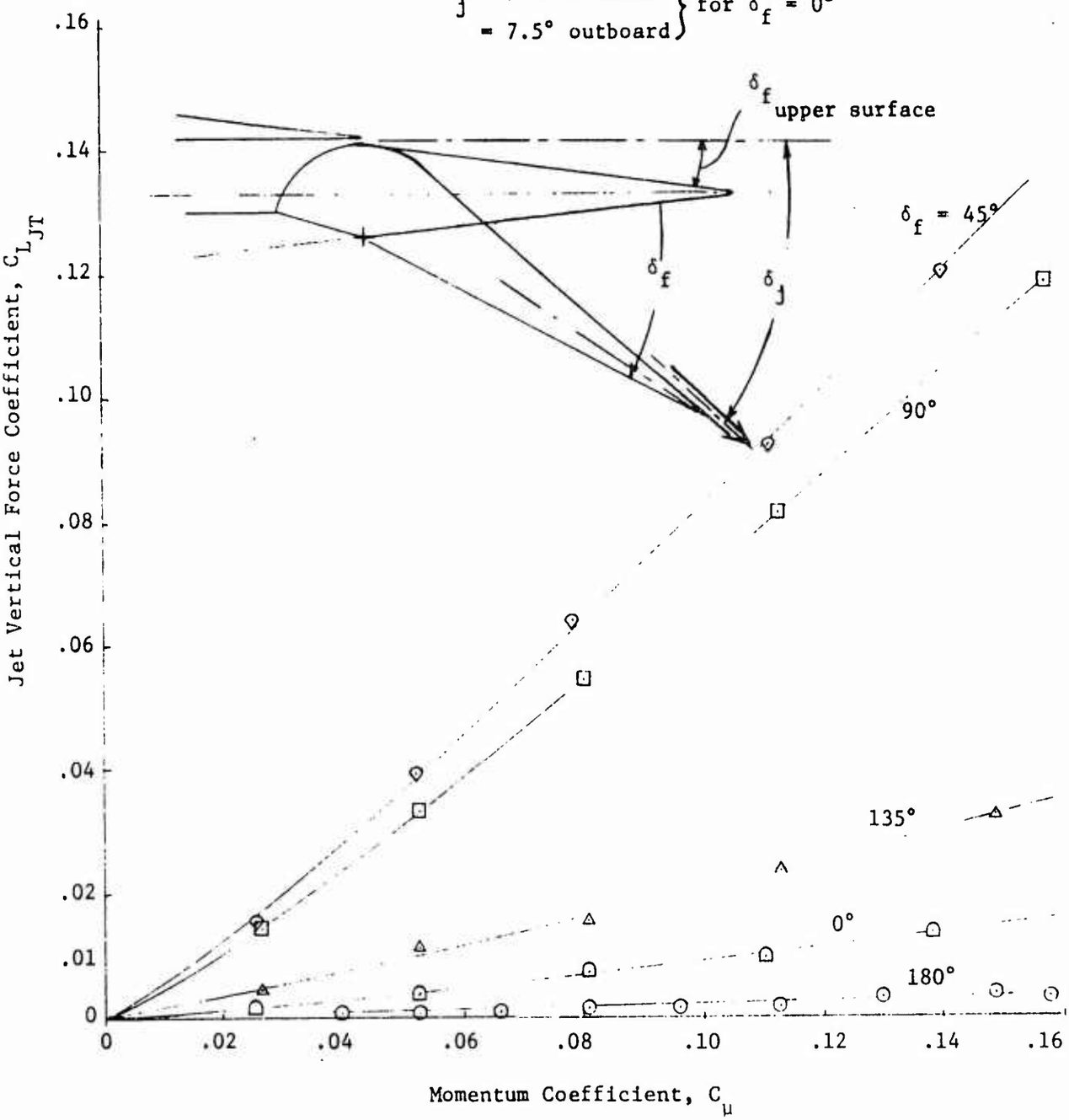

Figure 27 - Lift due to Vertical Component of Jet Thrust
($q_\infty = 0$)

Static Runs $q_\infty = 0$ $\alpha_{FRL} = -2°$, $\alpha_w = 0°$

Nondimensionalized by qS = 30 (10.2) = 306#

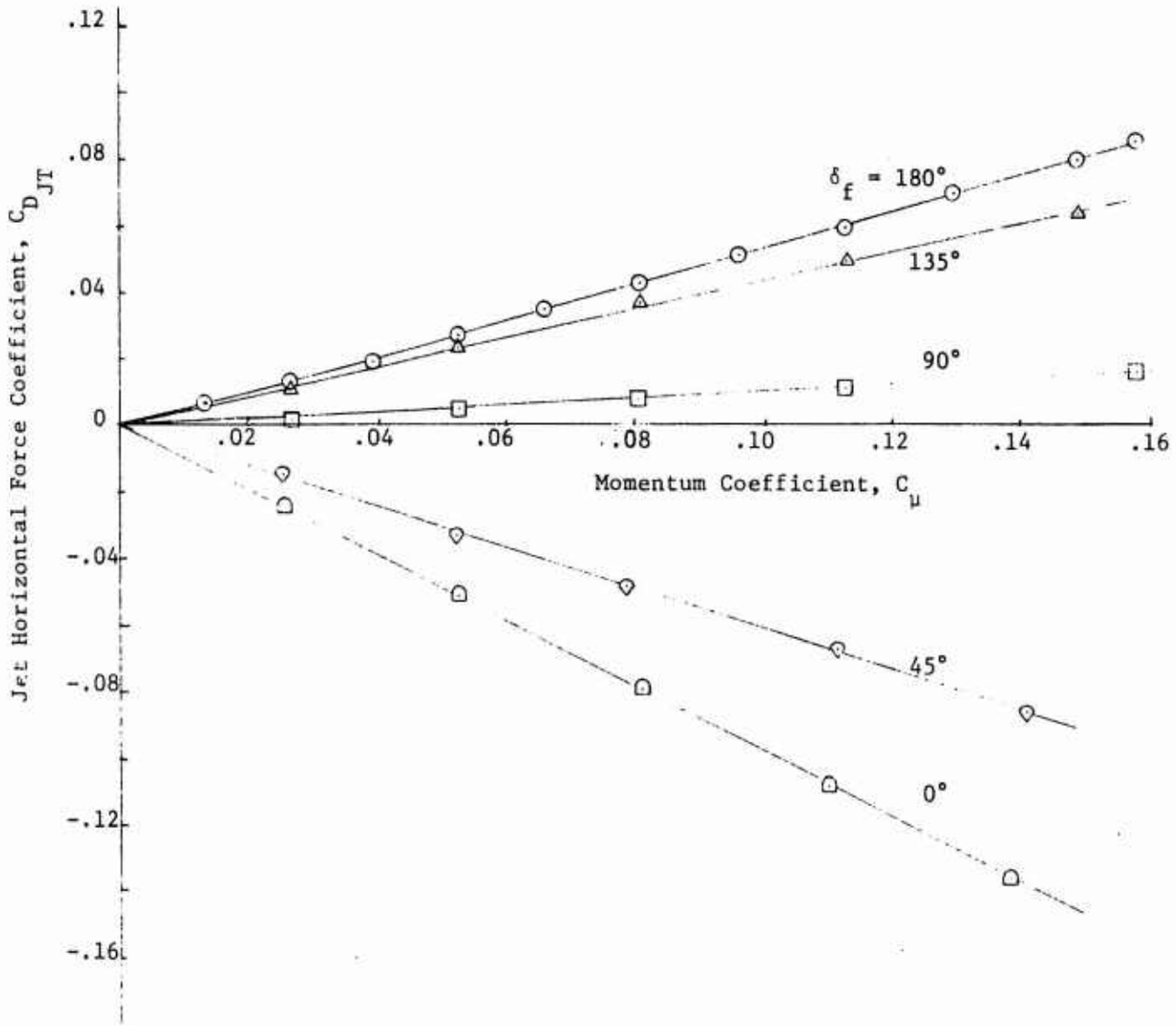

Figure 28 - Drag (or Thrust) due to Horizontal Component of Jet Thrust ($q_\infty = 0$)

Config. 3, $\delta_f = 180°$, $\delta_n = 30°$, $\delta_{n_o} = 0°$

No fences, Tail-off

	q	$R_e \times 10^{-6}$	Run
⊙	41	1.68	53
△	30	1.46	54
◇	20	1.19	55
□	10	0.85	56
⌂	5	0.60	57

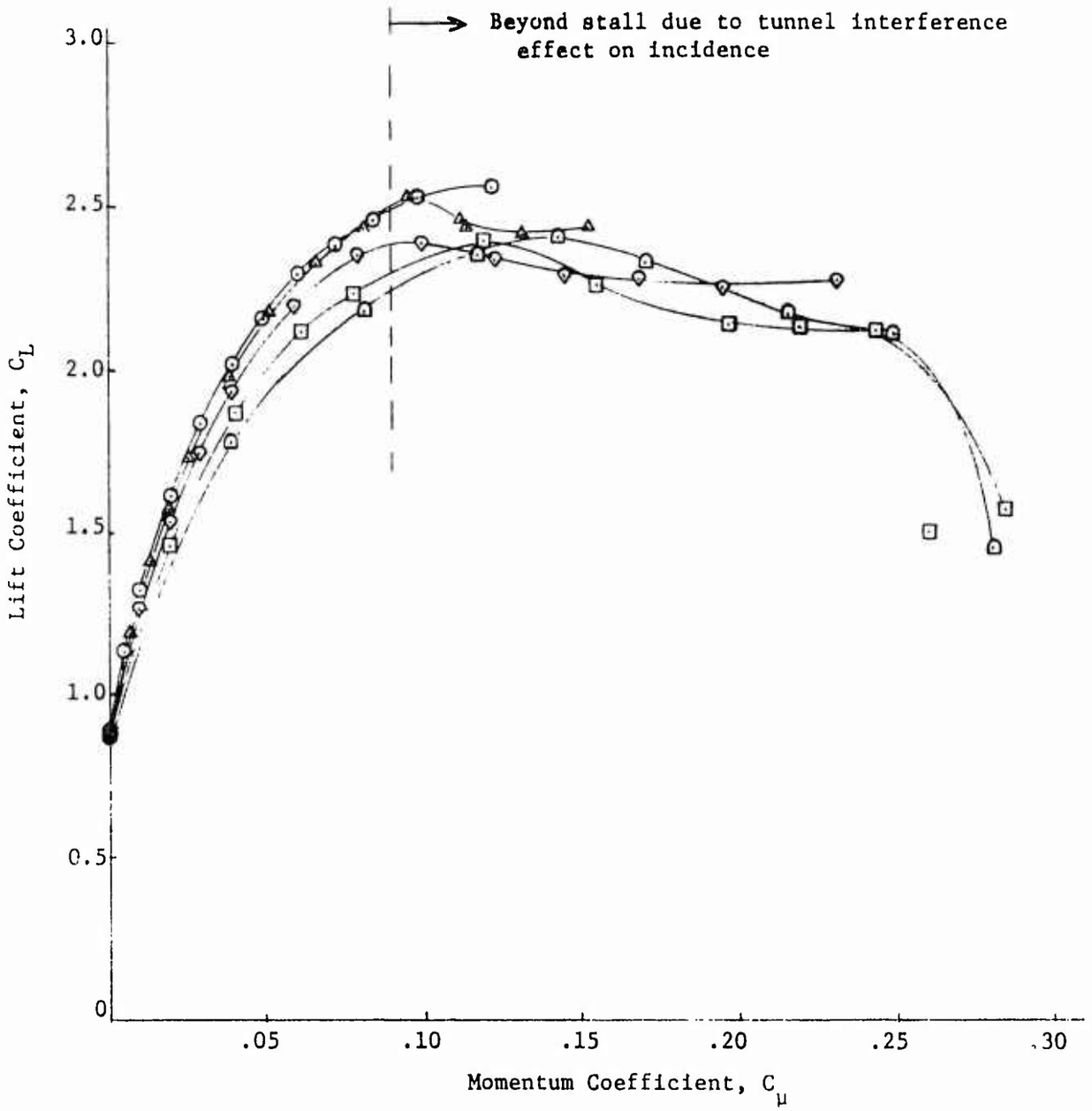

Figure 29 - Effect of Reynolds Number Variation on Lift

$\alpha_{FRL_{geo}} = 8°$

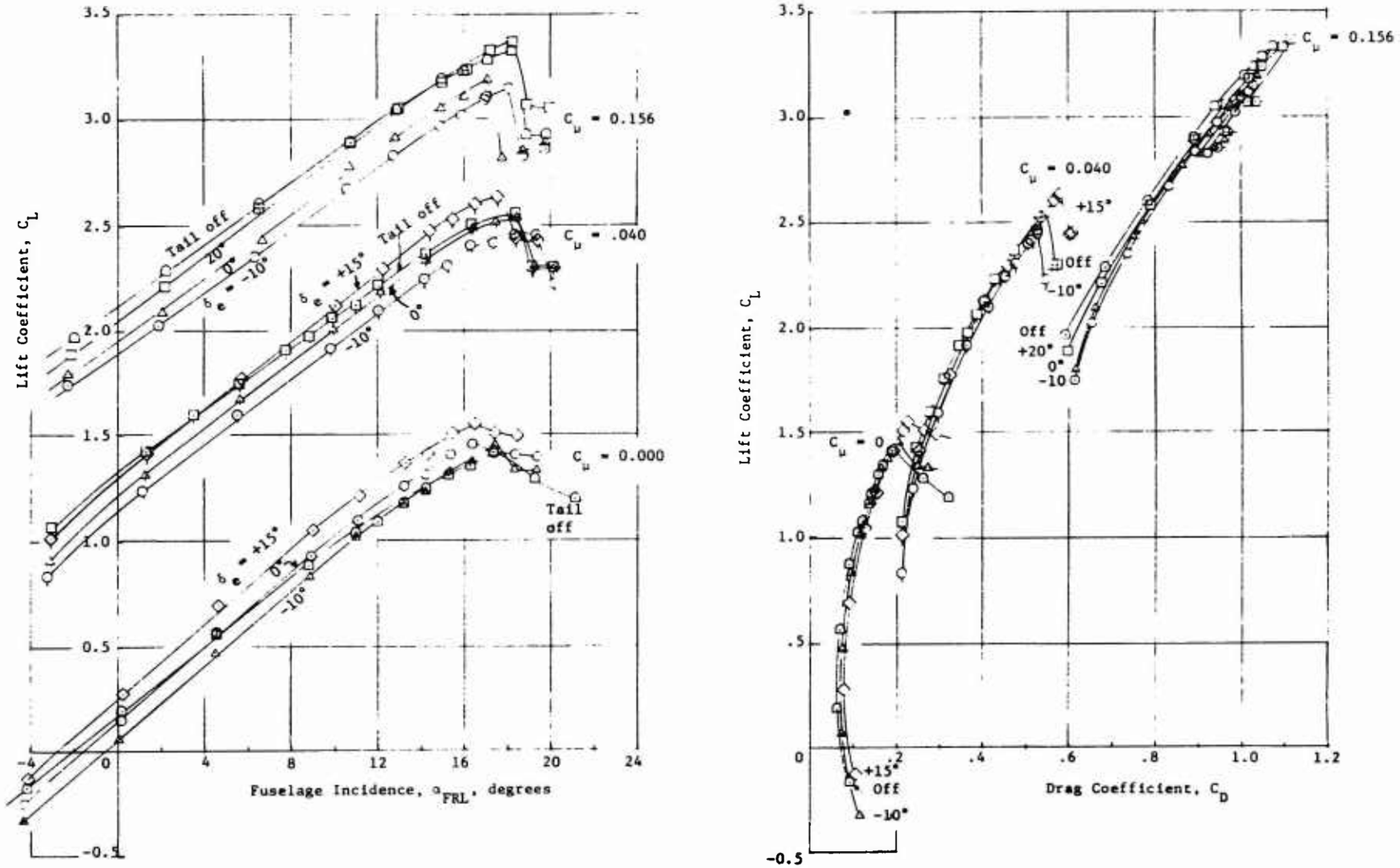

Figure 30 - Effect of Blowing on Tail-On Longitudinal Characteristics of Configuration 5 (δ_f = 180°, δ_n = 30°, δ_{n_o} = 10°, Fences, i_t = 0°)

a. Lift and Drag Coefficients

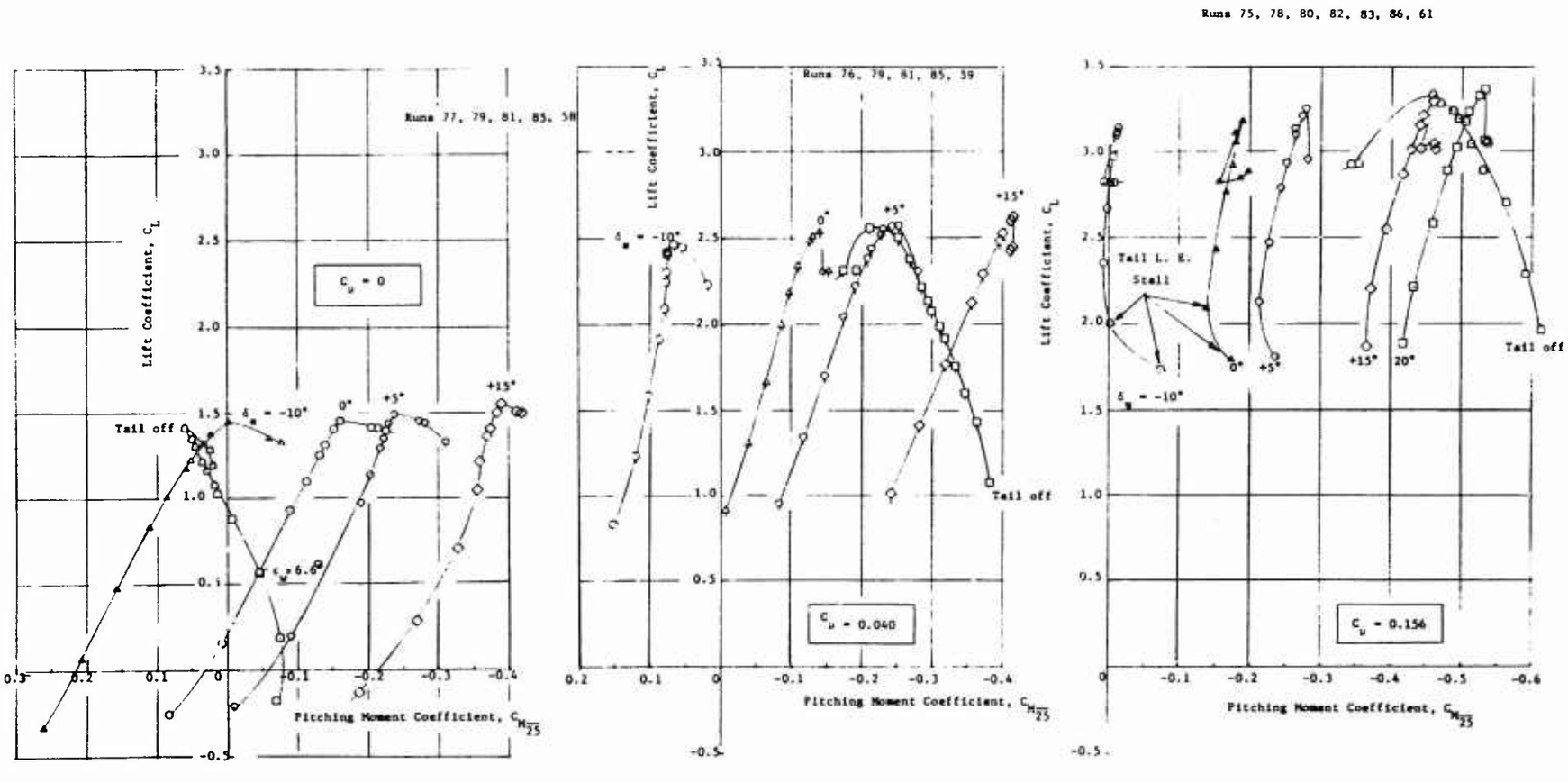

Figure 30 - (Concluded)
b. Pitching Moment Coefficient

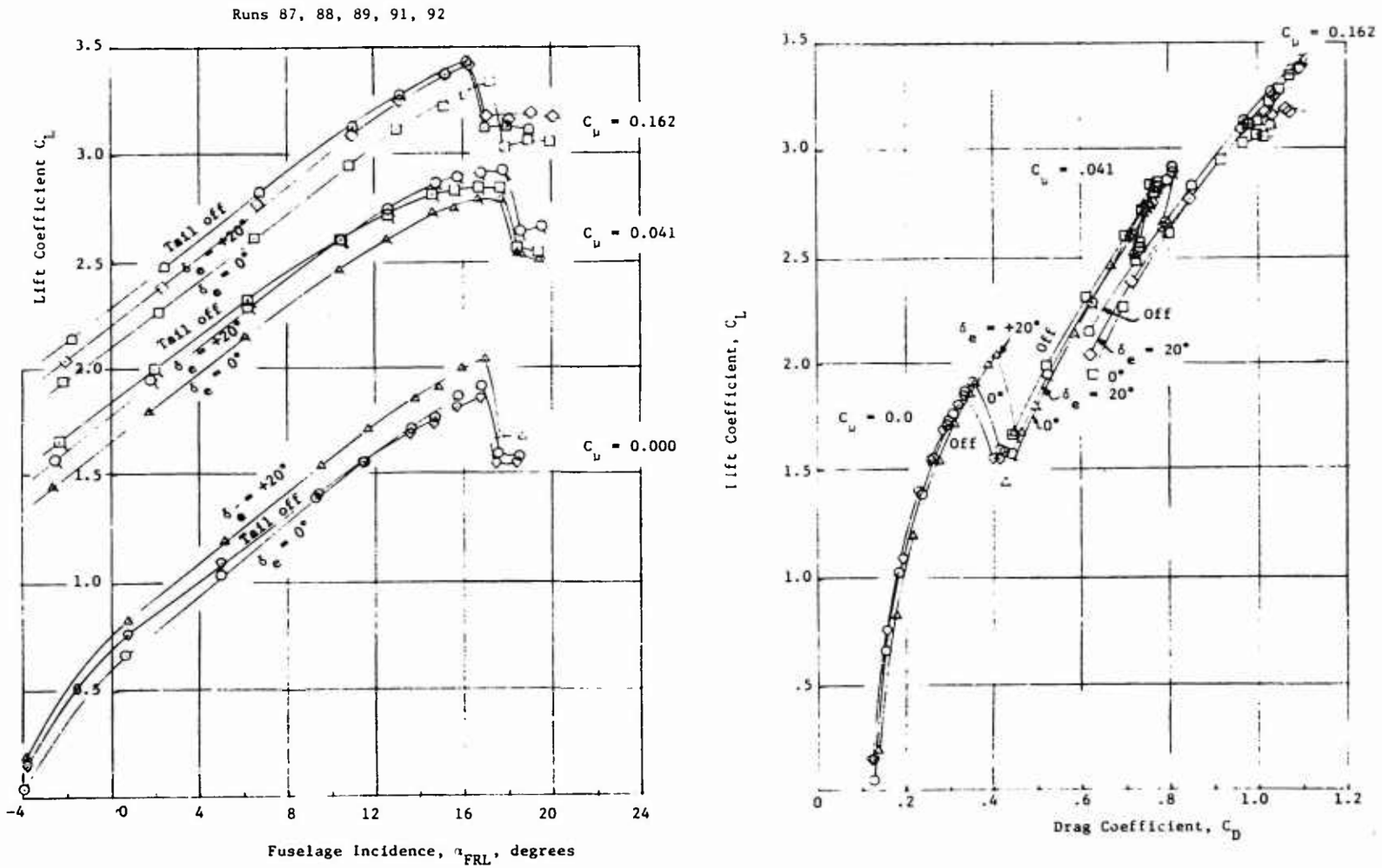

Figure 31 - Effect of Blowing on Tail-On Longitudinal Characteristics of Configuration 6 (δ_f = 90°, δ_n = 30°, δ_{n_o} = 10°, Fences, i_t = 0°)

a. Lift and Drag Coefficients

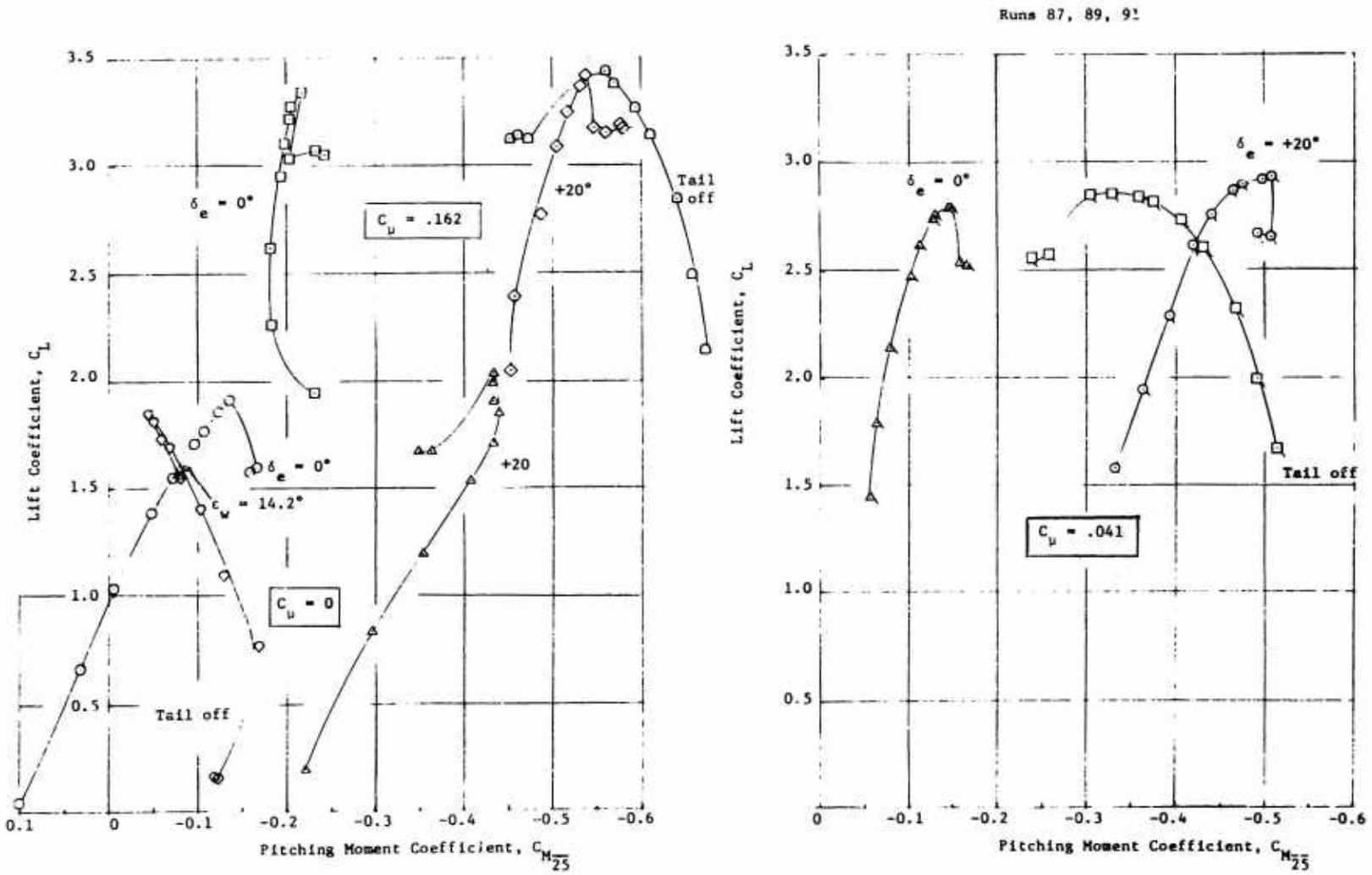

Figure 31 - (Concluded)

b. Pitching Moment Coefficient

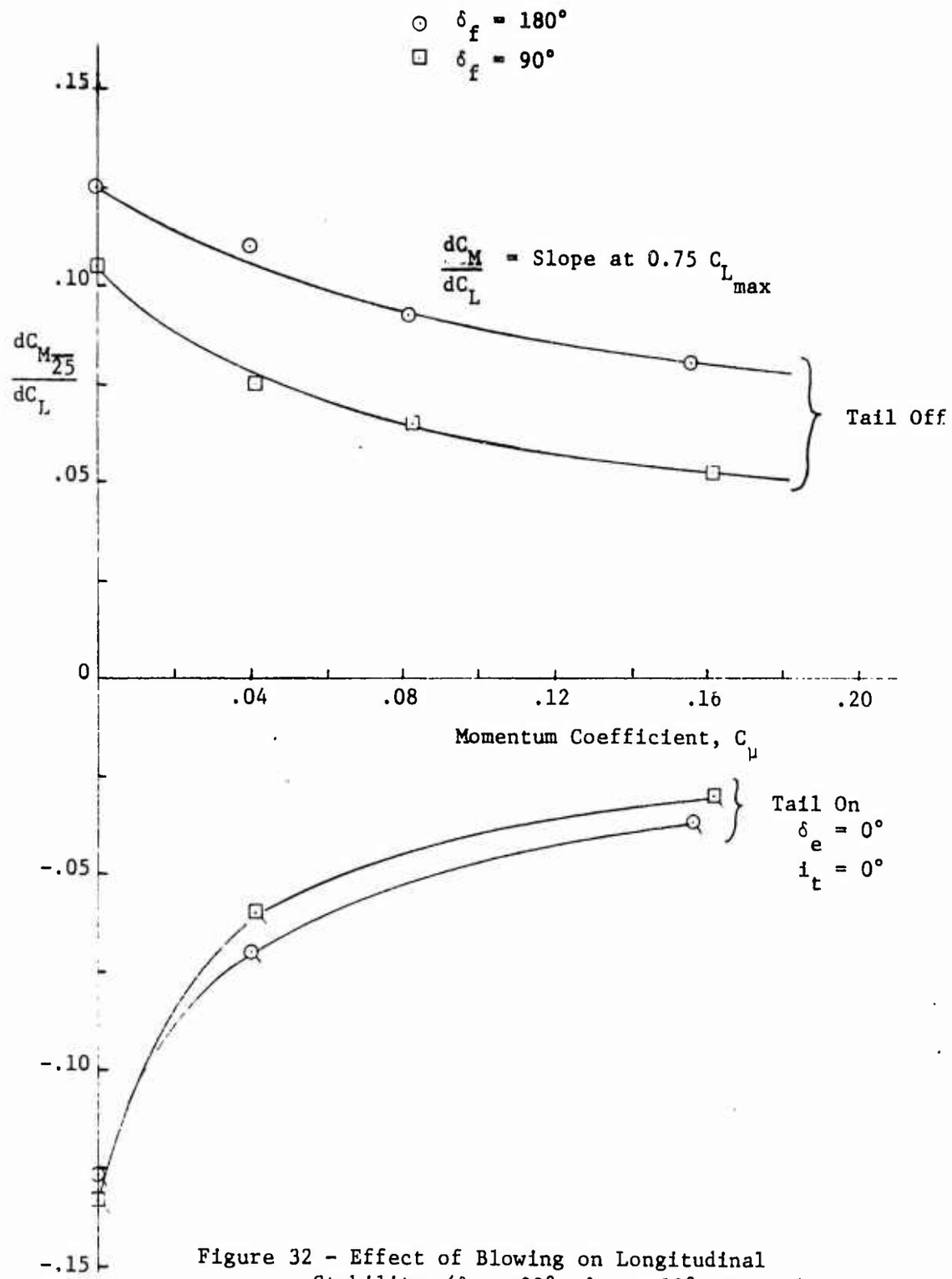

Figure 32 - Effect of Blowing on Longitudinal Stability (δ_n = 30°, δ_{n_o} = 10°, Fences)